University of Alberta

The Mid-Crust of the Western Slave Province - Geological Mapping, Geochemistry, and U-Pb Geochronology of the Forked Lake Area, Southwestern Slave Province, N.W.T.

by

Matthew James Perks

A thesis submitted to the Faculty of Graduate Studies and Research in partial fulfillment of the requirements for the degree Master of Science

Department of Earth and Atmospheric Sciences

Edmonton, Alberta

Fall 1997

National Library of Canada
Acquisitions and Bibliographic Services
395 Wellington Street
Ottawa ON K1A 0N4
Canada

Bibliothèque nationale du Canada
Acquisitions et services bibliographiques
395, rue Wellington
Ottawa ON K1A 0N4
Canada

Your file Votre référence

Our file Notre référence

The author has granted a non-exclusive licence allowing the National Library of Canada to reproduce, loan, distribute or sell copies of this thesis in microform, paper or electronic formats.

L'auteur a accordé une licence non exclusive permettant à la Bibliothèque nationale du Canada de reproduire, prêter, distribuer ou vendre des copies de cette thèse sous la forme de microfiche/film, de reproduction sur papier ou sur format électronique.

The author retains ownership of the copyright in this thesis. Neither the thesis nor substantial extracts from it may be printed or otherwise reproduced without the author's permission.

L'auteur conserve la propriété du droit d'auteur qui protège cette thèse. Ni la thèse ni des extraits substantiels de celle-ci ne doivent être imprimés ou autrement reproduits sans son autorisation.

0-612-22653-0

Canada

University of Alberta

Library Release Form

Name of Author: Matthew James Perks

Title of Thesis: The Mid-Crust of the Western Slave Province - Geological Mapping, Geochemistry, and U-Pb Geochronology of the Forked Lake Area, Southwestern Slave Province, N.W.T.

Degree: Master of Science

Year this Degree Granted: 1997

Permission is hereby granted to the University of Alberta Library to reproduce single copies of this thesis and to lend or sell such copies for private, scholarly, or scientific research purposes only.

The author reserves all other publication and other rights in association with the copyright in the thesis, and except as hereinbefore provided, neither the thesis nor any substantial portion thereof may be printed or otherwise reproduced in any form whatever without the author's prior written permission.

Matthew J Perks

33 Lea Vale Rd
Norton, Stourbridge
West Midlands
DY8-2AY
British Isles

Date: 30th September 1997

University of Alberta

Faculty of Graduate Studies and Research

The undersigned certify that they have read, and recommend to the Faculty of Graduate Studies and Research for acceptance, a thesis entitled The Mid-Crust of the Western Slave Province - Geological Mapping, Geochemistry and U-Pb Geochronology of the Forked Lake Area, Southwestern Slave Province, N.W.T submitted by Matthew James Perks in partial fulfillment of the requirements for the degree of Master of Science.

T. Chacko (co-supervisor)

R. A. Creaser (co-supervisor)

L. Heaman (committee member)

M.E. Evans (committee member)

Date 30th SEPTEMBER 1997

In memory of Lily Perks

"Each that we lose takes parts of us;
A crescent still abides,
Which like the moon, some turbid night,
Is summoned by the tides."
- Emily Dickinson

Plate 1. An aerial view of Forked Lake from the wing of a Cessna. The first camp-site is located on the knobby peninsula on the eastern shore of the lake (right side). The sky is fogged with smoke from local fires.

Abstract

From a rare exposure of granulite rocks in the Ghost domain of the Archean Slave Province, detailed mapping of the Forked Lake area revealed a circular pattern to the geology, a result of late-stage cross folding. When the effect of folding is removed, the area is seen to have been of a flat-lying sequence of orthogneisses and interlayered metasediments intruded by sheet-like bodies of opx-granite and K-feldspar megacrystic granite. U-Pb zircon geochronology on a megacrystic and an opx-granite yielded igneous ages of 2598 +6 -4 Ma and 2589 +3 -2 Ma, respectively, and analysis of metamorphic zircon from a mafic granulite yielded an age ca. 2592 Ma. The age of metamorphism is consistent with the age of intrusion of the granites, suggesting that magmatism and high-grade metamorphism were synchronous. Indeed, intrusion of these sheet-like bodies may have been at least partly responsible for advecting heat from deeper crustal levels and promoting granulite-facies metamorphism in the mid-crust.

Acknowledgments

Funding was provided by the Canadian Circumpolar Institute and by an N-SERC (Lithoprobe) grant to Dr. Thomas Chacko. I would like to thank Dr. Thomas Chacko for his guidance, wisdom, and inspiration throughout the project, and Dr. Robert Creaser for his constructive editorial critiques and the processing of the Sm/Nd samples. I am indebted to Dr. Larry Heaman for providing a valuable insight into the topic of U-Pb geochronology, and I am grateful for the assistance of Dr. Philippe Erdmer in the unraveling of the structural history of the Forked Lake area. Thanks also to Drs. John Henderson and Wouter Bleeker for providing me with a regional geological perspective of Forked Lake, and to Elena Kitova for her hours of tutelage and patience in both the clean laboratory and on the TIMS. This paper has also benefited from the advice and playful abuse of a number of fellow graduate students, including Darlene Atkinson, Suman De, Leslie-Ann Driver, Karen Fallas, Steven Grant, Dave Hills, Jochen Mezger, George Morris (estranged PostDoc), Pauline Orr, Dave Selby, and Taro Yamashita, and from the continued friendships of Kerrie-Ann Shannon and Donna Trickett. Thanks also to Rob L'Heureux for braving the bugs and bears of Forked Lake with me in a most admirable fashion, and I forgive him his French ancestry, and to Paul Wagner for convincing me to last out my first Edmonton winter. Finally, I would like to acknowledge the love and spiritual support of my parents, June and Trevor Perks, who got me to Canada in the first place, and to Rufus, the ginger monster, for chewing on my hand lens with such canine dedication.

Table of Contents

1 Introduction 1

2 Description of the Regional Field Area 8

2.0 Introduction 8

2.1 General Geology of the Slave Province 8

2.2 Previous Work on Slave Granulites 10

2.3 The Wijinnedi Lake Area 11

2.4 The Ghost Domain 11

3 Geology of the Forked Lake Structural Dome 16

3.0 Introduction 16

3.1 Physiography 17

3.2 General Geology 17

3.3 Early Tectono-Stratigraphic Assemblage 18

3.3.1 YKS Sediment 18

3.3.2 Metagranitoid Complex 20

3.4 The Late Plutonic Assemblage 23

3.5 Granulite-Facies Metamorphism 30

3.6 Comparison of the Geology 31

3.7 Geochemistry 32

3.7.1 Igneous Rocks 32

Metagranitoids / Late Granitoids /

Granitoid Classification / Mafic Granulite

3.7.2 Sedimentary Rocks 51

3.7.3 Nd Isotopic Data 52

4 Archean Deformation **56**

4.0 Introduction 56

4.1 Deformation of the Forked Lake Area (D_1 - D_5) 56

4.2 Comparison of the Structural Geology 63

5 U-Pb Zircon Geochronology **64**

5.0 Introduction 64

5.1 Analytical Procedure 65

Liberation, Abrasion, and Dissolution of Zircon/

Isotope Chemistry & TIMS

5.2 U-Pb Geochronology Results 67

5.2.1 Description of Zircon Populations 68

Megacrystic Granite / Opx-Granite /

Mafic Granulite / Tonalite

5.2.2 Concordia 69

Megacrystic Granite / Opx-Granite /

Mafic Granulite / Tonalite

5.3 Discussion of U-Pb Geochronology Results 80

6 Conclusions **84**

The Nature of the Deep Crust at FL /

Igneous and Metamorphic Relationships

Literature Cited **88**

Appendix A **94**

Appendix B **95**

List of Tables

Table		Page
1	Major oxide and trace element data	44-46
2	Alumina-Saturation Index, Mg number and Rb/Sr ratios	47
3	Forked Lake and Burwash/Walsh formation major element oxides	51
4	Sm/Nd isotopic data	55
5	U-Pb zircon results	78-79

List of Figures

Figure		Page
1a	Metamorphic map of the Slave Province	4
1b	Simplified geology of the Slave Province	4
2	Geology of the south-western Slave Province	5
3	Geology of the Wijinnedi Lake area	6
4	Aeromagnetic map of the Ghost domain	7
5	Geological map of the Forked Lake area	14-15
6	AFM diagram	36
7	Alumina-Saturation Index	36
8	IUGS granitoid classification	37
9	Harker diagrams	38
10	Granitoid trace-element discrimination diagrams	39
11a-c	Rare earth element plots	40
11d	Rare earth element plots	41
12a-b	Trace-element spider diagrams	42
12c-d	Trace-element spider diagrams	43
13a-b	Basalt trace-element discrimination diagrams	49
13c	Basalt trace-element discrimination diagrams	50
14	$\varepsilon Nd_{(T)}$ vs. time of crystallisation or deposition	54
15	Summary of the structural history of the FL area	59
16	Stereonet plot of the pole-to-plane of the strike-and-dips	60
17	Concordia diagram for megacrystic granite	76
18	Concordia diagram for opx-granite	76
19	Concordia diagram for mafic granulite	77
20	Concordia diagram for tonalite	77

List of Plates

Plate		Page
1	An aerial view of Forked Lake (see dedication page)	-
2	Satellite photograph of the Forked Lake area	13
3	Migmatitic paragneiss (metatexite)	26
4	Granitoid gneiss displaying characteristic compositional banding	26
5	Layered mafic granulite	27
6	Mafic granulite enclave disrupted by veins of opx-bearing melt	27
7	Ortho- and clinopyroxene-bearing leucosome	28
8	Alignment of K-feldspar megacrysts in megacrystic granite	28
9	An aerial view of the opx-granite, SW shore of Boomerang Lake	29
10	Pegmatite intruding brittle country rock	29
11	S_1, isoclinal folds (F_2) and regional schistosity (S_2)	61
12	Meter-length ductile shear zone in paragneiss	61
13	Brittle extension structure	62
14	Megacrystic granite zircon fractions	72
15	Opx-granite zircon fractions	73
16	Mafic granulite zircon fractions	74
17	Tonalite zircon fractions	75

Abbreviations

ASI	alumina-saturation index
bt	biotite
cpx	clinopyroxene
crd	cordierite
CSI	calcic saturation index
DD	Dauphinee domain
DM	depleted mantle
FL	Forked Lake
GD	Ghost domain
grt	garnet
hbl	hornblende
HD	Hinscliffe domain
HREE	heavy rare earth element
ICPMS	Ion-coupled plasma mass spectrometry
kfs	K-feldspar
LILE	large ion lithophile elements
LREE	light rare earth element
MORB	mid-ocean ridge basalt
pl	plagioclase
opx	orthopyroxene
PRB	Peninsular Ranges Batholith
P-T	pressure - temperature
qtz	quartz
REE	rare earth element
sil	sillimanite
SP	Slave Province
TIMS	thermal ionisation mass spectrometry
WD	Wijinnedi domain
XRF	x-ray diffraction
YKS	Yellowknife Supergroup

1. Introduction

The Archean Slave Province (SP) of NW Canada is characterised by widespread granitic magmatism and greenschist- to upper amphibolite-facies metamorphism (Fig. 1). These features testify to the presence of high crustal geothermal gradients during the Late Archean when much of the SP crust formed and stabilised. It is somewhat surprising, therefore, that the SP has fewer occurrences of granulite-facies rocks than most other Archean cratons (Padgham and Fyson 1992). For example, Thompson's (1978) metamorphic map of the SP (Fig. 1a) only identified two minor occurrences of granulite-facies rocks, and these are restricted to the SW part of the craton. A shallow level of erosion likely accounts for the paucity of granulite exposures in the SP but also implies that, for the most part, the deeper SP crust must be studied indirectly by geophysical techniques, or by utilising the geochemical signatures of granitoids as monitors of their lower crustal sources (Davis and Hegner 1992). It is highly desirable that data obtained from these indirect techniques be allied with direct observations made on actual exposures of deeper level rocks in the SP.

Recent mapping of the Wijinnedi Lake area in the SW SP by Henderson and Schaan (1993) (Fig. 2), discovered that an exposure of granulite-facies rocks, first recognised by Folinsbee (1940), is more extensive than previously thought. The granulite-facies terrane covers the southern third of the Wijinnedi Lake map south of Ghost Lake (Fig. 3), aptly christened the Ghost domain (GD) (Henderson and Schaan 1993). Composed of gneissic and foliated granitoids, migmatitic to diatexitic metasediments and, less commonly, metavolcanic rocks (Fig. 3), the rocks of the GD generally possess mineral assemblages diagnostic of granulite-facies metamorphism. However, the nature of the rocks directly south of the Wijinnedi Lake map have remained unknown. In a comparison between the geology and the aeromagnetic data for the region, Henderson and Chacko (1995) report a close correspondence between the exposure of granulite-facies rocks and a high relief aeromagnetic signature (Fig. 4). For

the most part, the surrounding region lacks any specific magnetic expression; the high relief expression of the GD, on the other hand, delineates a prominent 60 by 30 km, roughly triangular-shaped terrane (Fig. 4). A reconnaissance study by Henderson and Chacko (1995) confirmed the presence of granulite-facies assemblages along most of the northern, east central and southern parts of the terrane, leaving the SW side of the feature along which granulite-facies were not observed (Fig. 4). This interpretation is largely speculative, and by way of caution, may be misleading, as the true pattern of metamorphism in the GD might be misrepresented with such limited coverage of the feature to date. Field identification of granulite grade rocks included the recognition of macroscopic orthopyroxene in the orthogneisses, and where absent, was facilitated by the fresh green colour commonly displayed by granulite-facies rocks in hand sample.

The goal of this thesis is, in the first part, to investigate the nature of the deeper crust of the SW SP as exemplified by a representative portion of the GD. This is achieved by the presentation of a 1 : 25 000 geology map of the Forked Lake area (Fig. 5), with accompanying lithological and structural descriptions, incorporating whole-rock geochemical and Nd isotope data for selected rock-types. Forked Lake is located in the central GD and was targeted for this study for two reasons. Forked Lake was visited by Henderson and Chacko (1995), confirming the presence of granulite grade rocks in both sedimentary and orthopyroxene-bearing gneisses of the area, and identifying an exposure of megacrystic granite analogous to that mapped in the NW GD (Henderson and Schaan 1993). Thus the FL area can be considered as a lithologically representative portion of the GD. Secondly, the FL area also appears to be representative of the GD in a geophysical sense. The entire GD is characterised aeromagnetically by steep magnetic gradients arranged in a series of bull's-eyes (Fig. 4). The FL area is centered on, and is indeed the most prominent one, of these magnetic bull's-eyes. A major part of this thesis was to understand the geological cause for such a pattern as it may be representative of much of the deep crust in the western SP.

The second goal of this thesis is to examine the geological and geochronological relationship between igneous activity and high-grade metamorphism in the GD, investigated using U-Pb geochronology of zircon crystals by conventional thermal ionisation mass spectrometry. The single most important contribution of the geochronological study was to provide a constraint on the age of high-grade metamorphism in the SP and to compare this to the crystallisation age of the major igneous units. This was done to investigate whether the igneous intrusions provided the primary heat source for the metamorphism, or at the very least, augmented existing heat sources. The timing of metamorphism in the SP is generally considered coeval with a province-wide continental thickening event and associated voluminous intrusion of syn- to post-deformational granitoids. Numerous ages are available for the granitoids (e.g. van Breeman 1992) but nothing of similar fashion has been reported for the metamorphism. Reported here are crystallisation ages from a K-feldspar megacrystic granite and an opx-granite, and a preliminary age from a tonalite. Also reported is a preliminary metamorphic age from a mafic granulite. Because the protolith of the mafic granulite, a broadly basaltic composition igneous rock, contains negligible zircon, any zircon contained in the rock can reasonably be inferred to have grown during metamorphism (Percival and Krogh 1982; Heaman *et al.* 1986; Fraser *et al.* 1997). Therefore, U-Pb dating of this zircon provide a straight forward indication of the age of metamorphism without the complications that often arise when trying to determine the metamorphic age in rocks that have one or more populations of zircon inherited from their protolith.

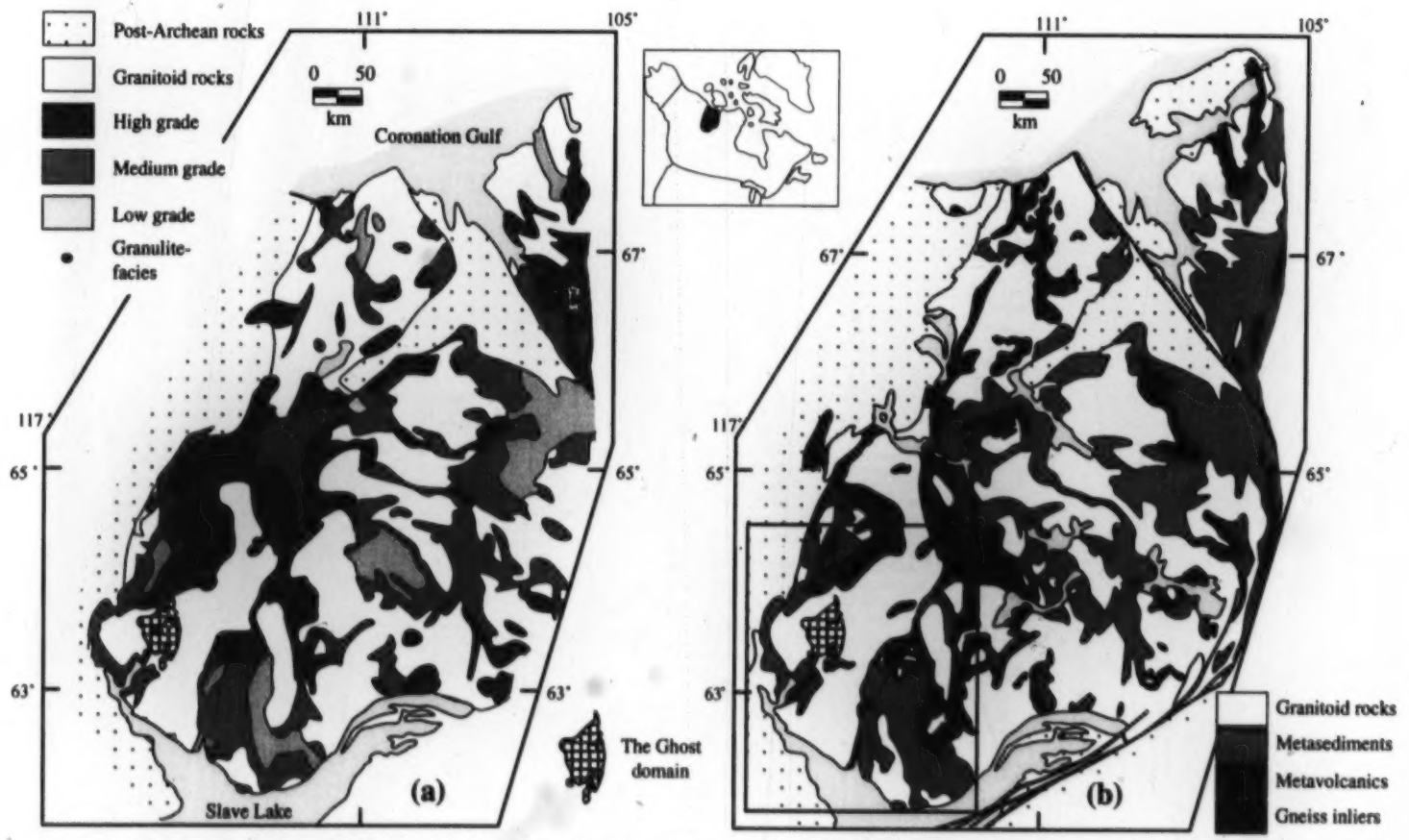

Figure 1. **(a)** Metamorphic map of the Slave Province (after Thompson 1978). Granulite locations from south to north: Forked Lake, Ghost Lake (Henderson and Schaan 1993), Daran Lake (Pehrsson *et al.* 1995), Winter Lake (Thompson 1978); **(b)** Simplified geology of the Slave Province, including location of major lakes in grey (after Hoffman 1989); black box shows approximate area covered by Figure 2. Ghost domain shown for reference in both cases. Location map is inset.

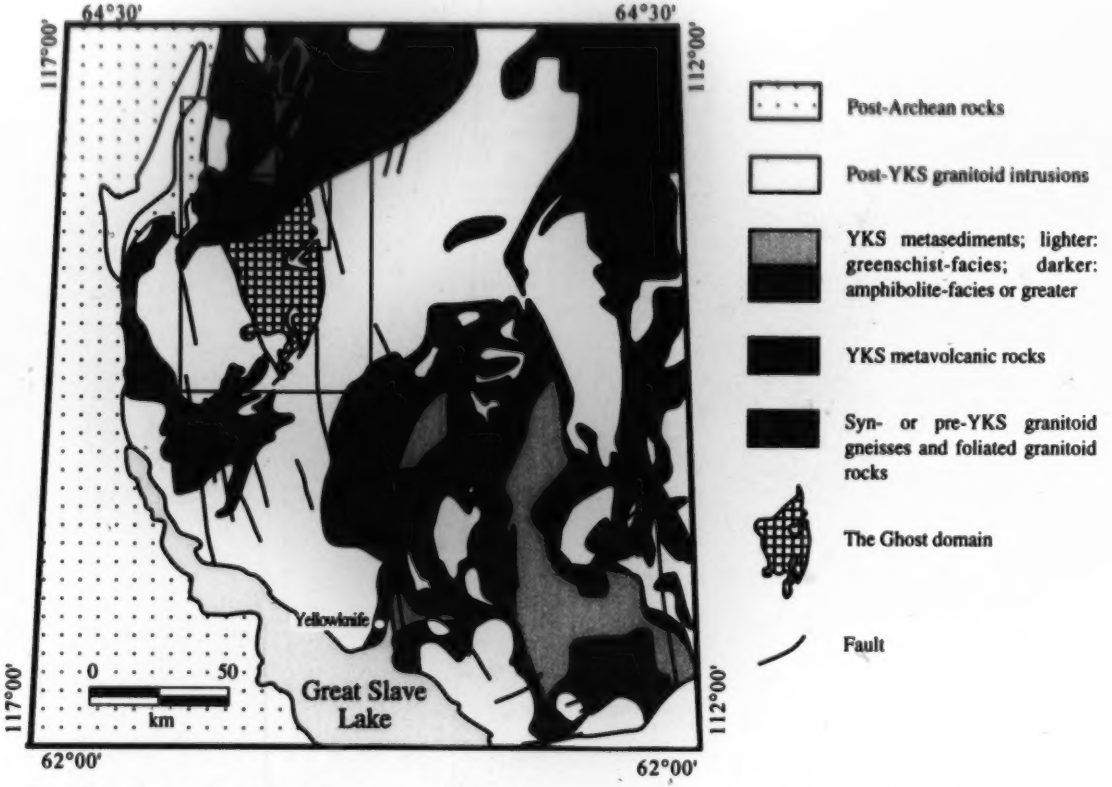

Figure 2. The south-western Slave Province (after Henderson and Schaan 1993), showing the location of the Ghost domain. Smaller black box corresponds to area covered by Figure 3, and larger black box to that of Figure 4.

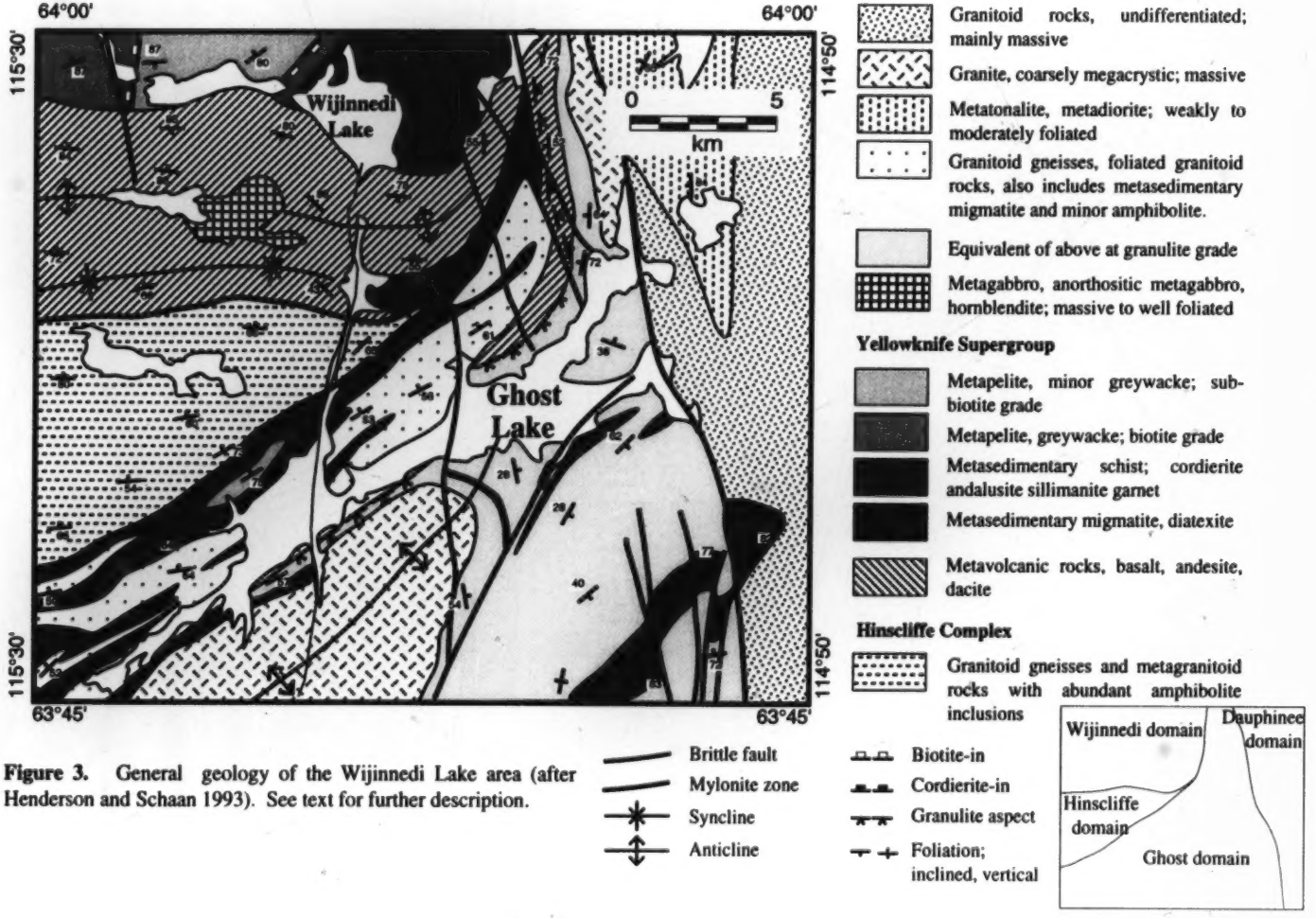

Figure 3. General geology of the Wijinnedi Lake area (after Henderson and Schaan 1993). See text for further description.

Figure 4. Aeromagnetic map of the roughly triangular-shaped Ghost domain (after Henderson and Chacko 1995). Heavy black line is the cataclastic shear zone that is the site of uplift. Dashed black line is the western edge of the Ghost domain. The location of outcrops seen in the course of the reconnaissance survey are shown with apparent presence (full circle) or absence (empty circle) of orthopyroxene.

2. Description of the Regional Field Area

2.0 Introduction

The purpose of this chapter is to place the FL area into its regional setting, first in context of the SP, and then in context of the Wijinnedi Lake and GD regions. The geology of the Wijinnedi Lake area is arguably a high-grade equivalent of the FL area. For the sake of brevity, however, the prefix 'meta,' indicating that a rock is a metamorphic equivalent of the original, will be omitted from the words volcanic rock and sediment, as all such supracrustal sequences within the SP are metamorphosed.

2.1 General Geology of the Slave Province

The SP is a relatively small (230 000 km^2) Late Archean craton, located in the NW corner of the Canadian Shield (Padgham and Fyson 1992). It displays broadly similar lithological, structural and metamorphic characteristics across the entire province. These features have produced a map pattern that is both bulbous and irregular (Fig. 1b; Thompson 1989). This same basic pattern is present in the metamorphic map, in which areas of greenschist-facies rocks surround lower to upper amphibolite-facies rocks in an irregular, crudely rhombic pattern (Fig.1a; Thompson 1978). The SP is essentially a granite-greenstone terrane, containing belts of tightly-folded, predominantly turbiditic sedimentary rocks (~30%) and subordinate volcanic rocks (~5%), wrapped around and extensively intruded by voluminous granitoid plutons (~65%). The greenstone units and most turbidites are grouped collectively in the 2710 - 2650 Ma Yellowknife Supergroup (YKS) (Henderson 1970), while the granitoids range in age from 2695 - 2580 Ma, evolving over time from older diorite-tonalite to younger syenogranite (Hill and Frith 1982). The granitoids further subdivide into pre-deformational (2695 - 2650 Ma) and syn- to post- deformational (2625 - 2580 Ma) plutons, the latter grouping making up ~80% of the total area (Fyson and Helmstaedt 1988; van Breeman *et al.* 1992).

The SP also contains a number of older high-grade gneiss inliers, predominantly in the upper amphibolite-facies, that are restricted to the western SP. These terranes may, in some cases, be contemporaneous high-grade equivalents of the granite-greenstone terrane, and in others, be older pre-YKS basement or tectonically juxtaposed crust. The older gneisses are an assortment of amphibolitic-tonalitic gneisses, massive tonalites, granitoids and related supracrustal rocks ranging in age from 3960 - 2840 Ma (Krogh and Gibbons 1978; Easton 1985; Bowring *et al.* 1989; Villeneuve *et al.* 1993). One of these gneisses, the Acasta gneiss, has acquired fame as the oldest known rock in the world, now significantly older than 4.0 Ga (Stern *et al.* 1997).

The apparent confinement of older material to the western portion of the SP, suggests a hidden complexity in the nature of the underlying crust in opposing halves of the craton, although as yet, the structural break between them remains undiscovered. This distinction may also be denoted in the trend and composition of the greenstone belts (Kusky 1989). Western and central belts run parallel in narrow N-S trends, whereas eastern belts trend NW-SE (Fig. 1b). The central N-S greenstone belt is coincident with a major Bouguer anomaly, to the west of which the volcanic rocks predominate over sediments, and to the east of which, sediments predominate over the volcanic rocks. The eastern belts also contain a larger proportion of felsic material than their western equivalents (Padgham 1985). This dichotomy in geological history is also inferred from a variety of laboratory results (Davis and Hegner 1992; Thorpe *et al.* 1992; van Breeman *et al.* 1992; Davis 1996). For example, Davis and Hegner (1992) use Sm-Nd systematics in post-deformational plutons to delineate a dividing line (~110°) either side of which the values of εNd differ significantly. Eastern plutons have positive εNd values suggesting juvenile crustal sources dominated by Late Archean crust, whereas western plutons possess negative εNd values indicating crustal sources dominated by Mid to Early Archean crust. In addition, Thorpe *et al.* (1992) proposed a Pb-Pb isotope boundary on the basis of Pb isotopic composition of volcanogenic-massive-sulphide deposits, broadly correlating to the work of Davis and Hegner and running approximately along longitude

112° (Fig. 1b). This evidence is in keeping with an accretionary history to the SP prior to the major continental collision event at the end of the Late Archean.

2.2 Previous Work On Slave Granulites

Folinsbee (1940) produced the first published report of granulite-facies rocks south of Ghost Lake, in a paper documenting the occurrence of gem-quality cordierite, or iolite, just south of Ghost Lake. The actual size of the granulite exposure remained unknown, however, until the much later work of Henderson and Schaan (1993) and Henderson (1994), despite previous mapping studies of the region by a number of workers (e.g. Lord 1942; Yardley 1949; Wright 1954). The late discovery of the GD was possibly because of the regional nature of these previous mapping projects. For example, Lord's map (1942) of the Snare River region includes the GD within a large expanse of undivided Archean granitoids. Wright (1954) commented on the highly complex terrane south of Ghost Lake that contrasted from other massive, homogeneous granitoid terranes in the SP. Robertson and Folinsbee (1973) document orthopyroxene in both the granite and metasediments south of Ghost Lake. The present study is catalysed by the work of Henderson and Chacko (1995), whose reconnaissance confirmed the southern continuation of the GD south of the Wijinnedi Lake area.

The apparent exposure of granulite-facies rocks in the SW SP is larger than originally realised. Other references to high-grade rocks in the area now indicate a much larger exposure, including reports by Thompson (1978) and Thompson *et al.* (1993, 1994) at Winter Lake, situated 125 km NE of Ghost Lake, and by Pehrsson and Beaumont-Smith (1994) and Pehrsson *et al.* (1995) in the Indin Lake supracrustal belt, and by Pehrsson and Chacko (1997) along a transect from Snare Lake to Winter Lake, due north of the GD. Only future work will delineate the true extent and nature of the granulite-facies exposure in the SW SP.

2.3 The Wijinnedi Lake Area

Henderson and Schaan (1993) and Henderson (1994) detail the geology of the Wijinnedi Lake area (Fig. 3). Summarised here are the salient points of these studies as deemed necessary background to the present study. The Wijinnedi Lake area is situated close to the SW margin of the SP, at the southern end of the Indin Lake supracrustal terrane, and at the northern end of an asymmetric block uplift as outlined by Henderson and Chacko (1995). The Wijinnedi Lake area was divided into four lithotectonic domains, the Wijinnedi (WD), Hinscliffe (HD), Ghost (GD) and Dauphinee (DD) domains, each possessing characteristic geology and bounded by prominent shear or fault zones. The metamorphic grade increases southwards through the terranes, from greenschist in the north to granulite in the south, highlighting an increase in depth facilitated by structural juxtaposition between the domains. Thus the WD, in the north, is the least deformed of the domains and is composed of a major mafic intrusive complex and YKS rocks. The HD is structurally below the WD and to the south, composed of granitoid gneisses and granitoid rocks, with a noted absence of any YKS rocks. The GD of Henderson and Schaan (1993), to the south and structurally below all other terranes, is the most heterogeneous and consists of the most highly deformed YKS rocks, as well as variably deformed and metamorphosed granitoid intrusive phases, and a major pluton of megacrystic granite (Fig. 3). The DD occurs along the eastern margin of the area, peripheral to the uplifted terrane to the west, predominately composed of massive granites. The bounding fault between the DD and the block uplift is a low grade cataclastic shear zone, in contrast to the ductile shear zones that form the boundaries of the other domains. This suggests that the other domain boundaries occurred earlier in the geological history when the crust was relatively hotter and more ductile.

2.4 The Ghost Domain

The GD is located in the SW SP, 160 km NNE of Yellowknife (Fig. 2), at the southern extremity of the Wijinnedi Lake area south of Ghost Lake. The GD is roughly

triangular in shape, a 60 by 30 km high-grade gneiss terrane; up to now it is the only significant area of granulite grade rocks in the SP. The GD is dominated by metamorphosed and foliated granitoid rocks and granitoid gneisses, and less commonly migmatitic to diatexitic sedimentary and, to a lesser extent, volcanic rocks. Henderson and Chacko (1995) report that the GD and HD orthogneiss complexes bear a strong resemblance to others elsewhere in the SP, such as the Cotter Hill Lake complex 20 km NNE of Ghost Lake (Frith 1993), and the Anton Complex north of Yellowknife, and Henderson and Schaan (1993) report a similarity to the Sleepy Dragon Complex, 100 km NE of Yellowknife (James and Mortensen 1992; Bleeker 1996). The rocks of the GD are considered deeper level equivalents of the granitoid gneisses and YKS rocks of the WD and HD respectively. P-T determinations calculated from Al-in-opx thermometry and garnet-plagioclase-orthopyroxene-quartz barometry support mid-crustal conditions of 6 - 7 kbar and 825 - 900°C for the northern edge of the GD (Chacko *et al.* 1995).

Plate 2. Satellite photograph of the Forked Lake area (highlighted box). Inferred Forked Lake (FLF) and Boomerang Lake faults (BLF).

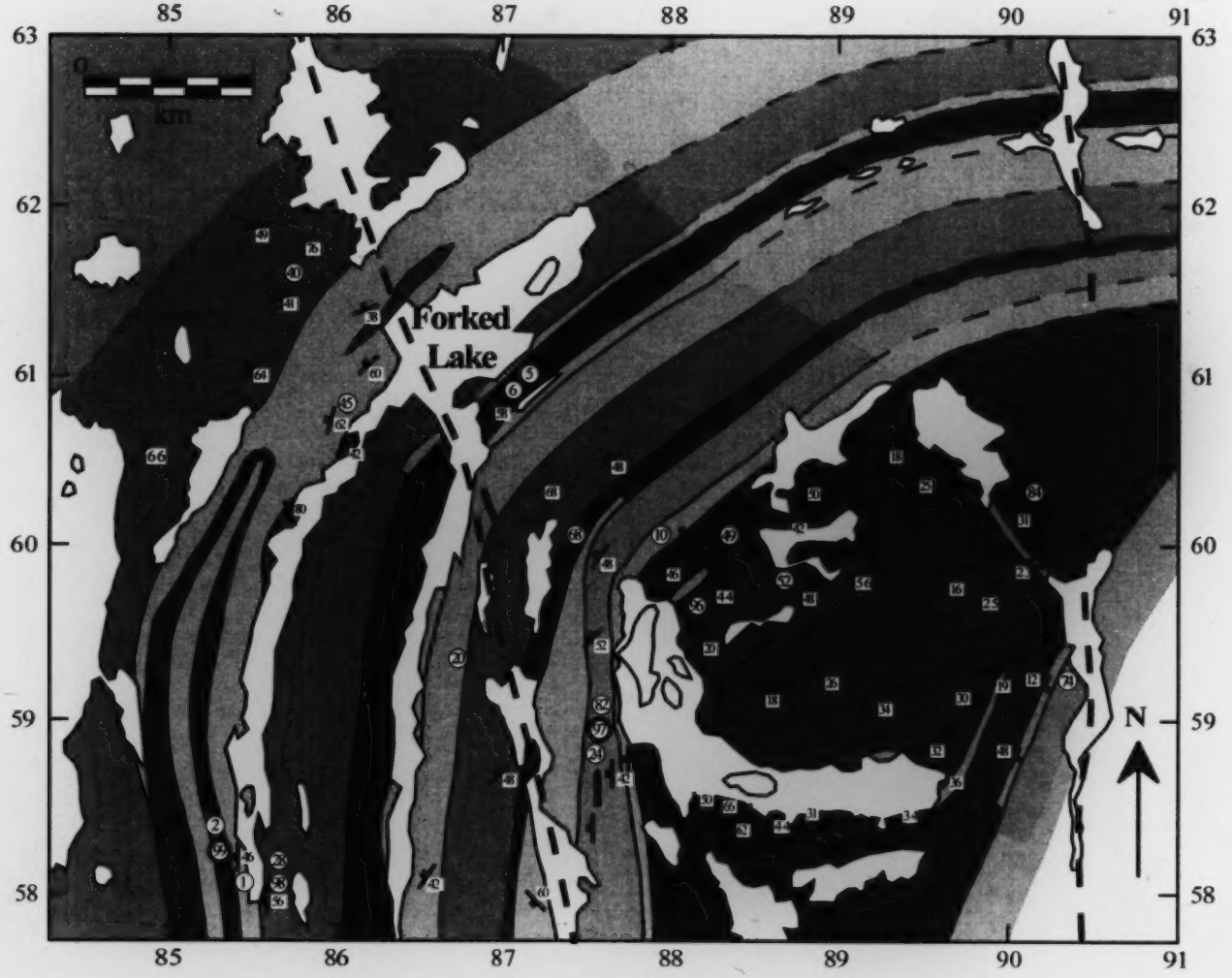
85
86
87
88
89
90
91
63
62
61
60
59
58
0
km
Forked
Lake
N

Figure 5. Geological map of the Forked Lake area (115°15' 63°40'). Lighter coloured region denotes area inferred from air photography, otherwise coverage was by 1 km spaced traverses. Blank regions within lakes correspond to unmapped islands. Grid reference locations for FL samples shown in Appendix A.

Map Key.

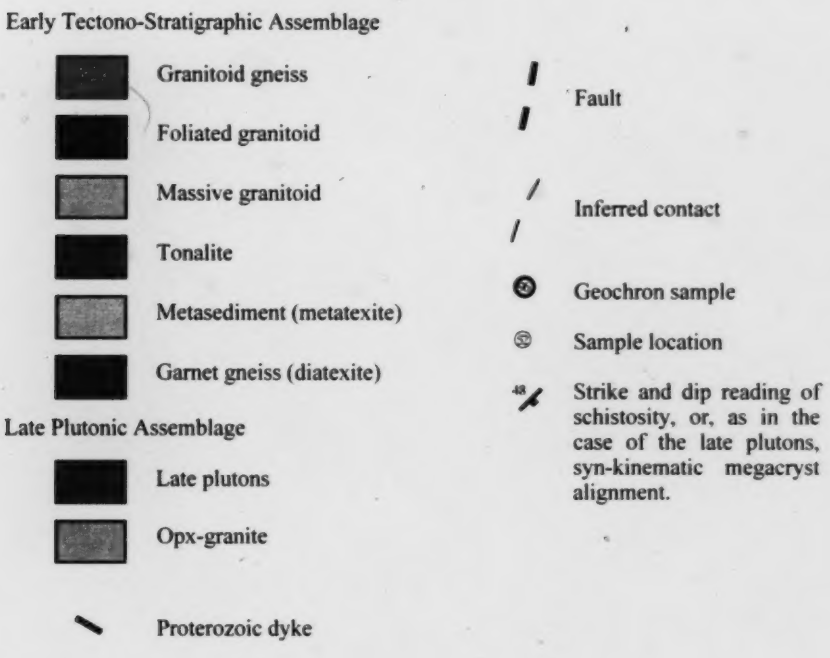

3. Geological Description of the Forked Lake Structural Dome

3.0 Introduction

This chapter describes the geology of the Forked Lake structural dome, commencing with a description of the physiography and geology of the area, and concluding with a report on the geochemistry of FL samples. The geological units are currently tilted as a result of late Type 1 interference folding, leading to the formation of a structural dome now truncated by the present erosion surface. Referral to the geological map of the FL area can be made throughout this section by turning to Fig. 5. The FL map was constructed over a four week period during the summer of 1995, and again, for one week, in 1996. Travel to the region was by float plane, and camps were kept on the shores of Forked Lake (867 - 609; Plate 1) and Boomerang Lake (877 - 589; Plate 9). Traverse was by foot, although a zodiac inflatable boat proved most useful on Forked Lake. The resulting map covers an area of approximately 25 km^2, on a scale of 1 : 25000. The map focuses on the western slope and crest of the dome, and the area to the north, although largely unvisited, is inferred from convincing air photography evidence (Plate 2). The eastern and southern parts of the dome were not visited nor could the geology of these areas be determined unambiguously from air photography evidence. However, according to the recognition of opx-granite on the opposing side of the dome, taken with the recorded pattern of strike and dip variations and the aeromagnetic bull's-eye pattern, and some musing over the air photography (Plate 2), there is supportable evidence towards a dome structure in the area. The author suggests that the geographical name 'Forked Lake' remains in any future work, as it is a direct derivative from the local Dogrib language (Ti ts'e go ti) (Aaron Herter, pers. comm., 1995). Boomerang Lake, on the other hand, was named by the author for convenience and the name need not be retained in the literature.

3.1 Physiography

The aeromagnetic bull's-eye expression of the FL area is mirrored in both the topography (Plate 2) and geology of the area (Fig. 5). The quartzofeldspathic gneisses and massive igneous rocks of the FL area lead to a rugged and undulating relief, composed of bare rocky ridges commonly rising abruptly above innumerable, intervening muskegs and lakes. The ridges usually follow the relatively resistant orthogneisses, while the stretches of muskeg and long narrow lakes correspond to less resistant paragneisses or to suspected faults. For example, the long prongs of Forked Lake form along belts of paragneiss, while a fault controls the bridge of the fork, depicted by a string of lakes trending NW-SE. Forked Lake, particularly, is connected to a series of lakes to the south, offering increased mobility around the area by boat. The topography of the central part of the area, however, is noted for its absence of lakes, and, because of its predominantly igneous nature, it is generally flatter and more hummocky than the outerlying area. A series of lakes, however, delineate the border of the igneous and metagranitoid units, the largest of which is the prominently right-angled Boomerang Lake, to the south. This, and other similar lakes close to the central region, may be exploiting brittle weaknesses created at the crest of the dome, especially at the contact between the contrasting rock-types, or by the presence of underlying sedimentary units.

The FL area is moderately well-timbered, especially where underlain by sedimentary and volcanic rocks, and also along the eastern extremity of the map area, where a thick bushy strand of conifers and birch prevails. The majority of the mapping site, however, is relatively sparsely timbered compared to adjacent forests, attributable to a series of fires that swept through the area in the early nineteen-seventies. In places, the fires have resulted in large areas of lichen-free exposure.

3.2 General Geology

The geology of the Forked Lake area is exposed in a late-stage dome structure. When the effects of the doming are removed, the geology is composed of a variety of

flat-lying units, within which are identified two contrasting rock associations, namely an early tectono-stratigraphic assemblage and a late plutonic assemblage. The early tectono-stratigraphic assemblage is composed of a supracrustal sequence of migmatised aluminous greywackes, with a subordinate psammitic component, intercalated with a variety of metagranitoids. Although subordinate to the metagranitoids, the sedimentary units are more abundant than indicated by the reconnaissance study of Henderson and Chacko (1995). The late plutonic assemblage, on the other hand, comprises a variety of granitic units exhibiting unequivocal evidence of intrusion into the former. This younger assemblage most likely intruded as sills, as exemplified by a sill of opx-granite on the western flank of Boomerang Lake (Fig. 5). The bulk of the plutons are exposed in the centre of the dome, and were at the base of the exposed section prior to doming. Thus the current exposure of the late plutonic assemblage in the GD may be controlled by later fold trends. For example, the megacrystic granite in the N GD (Henderson and Schaan 1993), which is of similar age (Villeneuve and van Breeman 1994), is exposed at the centre of a late antiform.

The only other rock-types in the area, which are unrelated to the Late Archean tectonothermal event, are the widespread intrusion of numerous diabase dykes that transect the whole Slave Province, in the FL area these range in size from decimetre- to up to 15 metre scale features. These dykes are correlative with the Proterozoic Indin dykes that traverse the SP in a NNW-trend. However, some dykes may be correlative with the rarer Mackenzie dyke swarm, that traverses the SP on a ENE trend.

3.3 Early Tectono-Stratigraphic Assemblage

3.3.1 YKS Sediment

The YKS sediments of the FL area are migmatised aluminous greywackes with a minor Fe-iron rich psammitic component that is restricted to occasional enclaves and layers. The migmatites occur in two textural forms. The term metatexite, following the

definition proposed by Brown (1973), "is a rock produced by metatexis and in which the migmatitic banding is evident." "Metatexis is the process of segregation (usually of quartz and feldspar) by metamorphic differentiation and partial fusion," (p. 374). The term diatexite of Brown (1973), on the other hand, refers to "a rock produced by diatexis and in which there is no continuous migmatitic banding." "Diatexis is high-grade anatexis in which fusion may be complete," (p. 375).

The metatexite is by far the most common textural form, characterised by a medium to coarse grained generally migmatitic rock consisting of a rusty brown weathered paleosome, though dark when fresh, and white trondhjemitic peraluminous leucosomes, sometimes with observable mantling melanosomes (Plate 3). The leucosome fraction normally consists of 2 - 10% of the total volume, containing large red garnets (2 - 5 cm), considered to be liberates from the paleosome rather than melt phases. The leucosome is parallel to the regional schistosity and usually only a few centimetres in thickness; the individual layers often discontinuous, being more in the nature of elongate lenses. The leucosome fraction sometimes reaches ~40% by volume. However, these larger bodies contain few garnets and occasional slivers of rotated sediment, raising suspicions that they represent local melt injection, rather than in-situ melt accumulation. Although garnet is generally widespread in the paleosome, in places it is absent, perhaps reflecting original compositional variations within the protolith. The macroscopic porphyroblasts of cordierite (3 - 6 cm), on the other hand, occur sporadically, but once a candidate has been discovered, cordierite is readily distinguished from quartz by its distinctive purple/bluish colour. No gem quality cordierite was observed. In contrast to the mineralogy of the greywackes, the psammitic enclaves rarely melt, possessing a refractory composition with abundant quartz, subordinate plagioclase, orthopyroxene, clinopyroxene, biotite and hornblende.

Several belts of migmatites were mapped on the western side of the dome, but sediments also occur as large rafts in the late plutonic assemblage of the core, and as abundant smaller enclaves. In the N GD a transition from metatexite through diatexite to

a hybrid granite-sediment rock was observed towards a pluton (Chacko, pers. comm., 1994). In the FL area, rafts and fragments of diatexite are observed occasionally within the core or close to igneous bodies. The identification of diatexite, however, is sometimes difficult, as it broadly resembles the metagranitoids. In general, however, the diatexites are more leucocratic and heterogeneous than the granitoids, and possess a distinctive texture and are commonly garnetiferous. For example, the garnet gneiss unit (Fig. 5) is interpreted as a diatexite, a consequence of melting and hybridisation between sediment and granitoid gneiss neighbours. The unit contains garnet and orthopyroxene segregations, numerous sweats of large red garnets in disbanded array, and frequent tiny garnets in a quartz, plagioclase, and biotite groundmass. Mafic segregations were also seen at a diatexite within the late plutonic assemblage, as grt-bt-qtz schlieren, and may represent the remains of more ferromagnesium rich portions of the original sediment.

One small, possible metamorphosed banded iron formation (879 - 601) was observed, associated with quartz veining, as an outcrop-sized enclave within a metasedimentary unit (Table 1). The rock was severely rusted and contained predominantly garnet and clinopyroxene, with interstitial quartz.

3.3.2 Metagranitoid Complex

The metagranitoids are considered high-grade equivalents of the HD, which is interpreted as an intrusive complex (Henderson & Schaan 1993) and synchronous to the age of YKS volcanism (Villeneuve and van Breeman 1994). The metagranitoids and HD probably represent a magma chamber for the volcanic rocks. In the field, the metagranitoids do not resemble volcanic rocks, they are massive units with no gradations in composition across their exposure, and may have been magmatically or tectonically intercalated within the supracrustal sequence (Fig. 5). The metagranitoids are divisible by textural characteristics into four rock-types, namely a massive and a foliated granitoid, a granitoid gneiss, and a tonalite. Garnets occur locally in the granitoids where hybridisation has taken place along the borders with sediments, as do sediment enclaves.

Dispersed within the metagranitoids are numerous blocks or enclaves of mafic granulite, in places observed as layers concordant to the strike of the regional schistosity.

Given the variations of rock-type within the complex, it must not have crystallised as one simple foliated body, but resulted from the multiple injection or ejection of numerous granitoid sheets. In this intrusive scenario, the metagranitoids are held responsible for the mechanical break-up of the original supracrustal sequence. The metagranitoid complex thus represents a prolonged activity of magmatism prior to the development of peak granulite-facies metamorphism, but synchronous with or subsequent to the deposition of the YKS. Alternatively, the metagranitoid complex may have been tectonically interleaved as large sill-like bodies within the sediments by thrusting.

The nature of the metagranitoids is as follows. The foliated granitoid gneiss is a medium to coarse grained rock possessing a characteristic foliation expressed in the alignment of macroscopic orthopyroxene. The presence of weathering orthopyroxene lends a distinctive orange hue to an otherwise pale white weathering surface. Where fresh, the foliated granitoid is characteristically dark green. Mineralogically, it contains quartz, K-feldspar, subordinate plagioclase, pyroxene, biotite, and sometimes hornblende. Two belts of foliated granitoid were mapped, one surrounding the core and one running between the two prongs of Forked Lake. Mafic enclaves are commonly dispersed throughout the unit. Furthermore, on the southern shore of Boomerang Lake (881 - 585), a unique exposure of strongly mafic enclaves was recorded, with coarse orthopyroxene and clinopyroxene forming the predominant minerals, with negligible plagioclase and hornblende. These enclaves formed orbicular pods, some 50 cm in diameter, containing prominent rims, 5 cm thick, with orthopyroxene rimming a clinopyroxene and plagioclase core.

The massive granitoid is an even medium grained rock, weathering with a pale purplish white hue. Mineralogically it contains a dominant felsic mineralogy of quartz, plagioclase and K-feldspar, with a mafic component of orthopyroxene and biotite. The texture is massive, implying the homogeneous appearance of the rock and absence of all

but a faint foliation. The lack of a pronounced foliation, that distinguish it from the other bodies in the complex, may in part be a reflection of its smaller mafic component. One unit of massive granitoid was mapped, with an approximate true thickness of 193 m, forming a prominent ridge on the eastern shore of the east prong of Forked Lake (Fig. 5).

The tonalite is a medium grained, pale white weathering rock, containing two phases. The first, a felsic component composed of quartz and plagioclase with small amounts of biotite, contains blocks or inclusions of the second, a mafic component constituted of quartz, plagioclase, biotite, ortho- and clinopyroxene. The mafic phase possesses a faint banding on a 10 cm scale. The tonalite exhibits only a faint foliation, expressed by biotite, and contains the occasional mafic enclave. Only one sill of the tonalite was mapped, possibly isoclinally folded, within a sediment unit on the SW shore of Forked Lake. The tonalite was not a melt component of the sediments, it is intruded by trondhjemitic leucosome traceable to the migmatised sediment along its border, and also contains enclaves of sediment presumably incorporated prior to metamorphism.

The granitoid gneiss is an even medium to coarse grained rock that possesses a characteristic banding or layering on a decimetre-scale, sometimes occurring sparsely or disrupted (Plate 4). The rock has a typically pinkish buff to buff weathered colour, and dark green to yellow brown fresh colour where at granulite grade. The granitoid gneisses are moderately heterogeneous in composition, because of their mineralogical banding, and express a compositional variation ranging from granodiorite to tonalitic portions. Mineralogically, the granitoid gneiss contains varying proportions of quartz, plagioclase, K-feldspar, pyroxene, hornblende, and biotite. Three granitoid gneiss belts were mapped, usually forming ridges or high ground.

The mafic granulites are fine to coarse grained segregations with a mineralogy of varying proportions of hornblende, biotite, ortho- and/or clinopyroxene, and plagioclase, although hornblende predominates over pyroxene, and ortho- over clinopyroxene. Many of the mafic layers and enclaves show signs of melting, as does the adjacent gneiss, disrupted by a network of sweats, lenses, and veins of melt, often containing macroscopic

ortho- and clinopyroxene (Plates 5, 6). The occurrence of macroscopic pyroxene is illustrated most impressively on the SW shore of Boomerang Lake (878 - 587), where 2 - 5 cm pyroxenes occur prominently within these sweats (Plate 7). The presence of melt may have increased migration rates of elements and thereby encouraging the growth of large crystals locally within the sweats. In some places metre-scale layers of mafic granulite are traced out along strike into disrupted mafic blocks and desegregated enclaves, and enclaves are generally dispersed throughout the metagranitoids. This field relationship is reminiscent of the HD (Henderson and Schaan 1993), where the enclaves are interpreted as the remnants of mafic dykes associated with YKS volcanism, since transposed, metamorphosed and broken up by deformation and associated melting. A small occurrence of coarse metadiorite enclaves (878 - 588), the only location where these were observed, may represent a rarely seen phase or deeper-level equivalent of the mafic dykes.

3.4 The Late Plutonic Assemblage

The late plutonic assemblage is composed of a variety of peraluminous granitoids, namely opx-, leuco-, garnet-, and megacrystic granites. The opx-granite occurs as a prominent sill intruded concordant to the regional schistosity developed within the early tectono-stratigraphic assemblage, whereas the other units are exposed within the centre of the map area corresponding to the low relief magnetic core of the aeromagnetic bull's-eye. These central units occur in a chaotic outcrop pattern, in many respects like a 'lithological oatmeal.' The scale of mapping, however, was not detailed enough to warrant the delineation of the complex outcrop pattern of the central region onto a map. However, it was noted that the occurrence of leucogranite is restricted to the NW (887 - 599), garnet granite is most abundant in the east, and the megacrystic granite occurs to the west and east, but is eclipsed in the west by a high proportion of pegmatite. Due to increased ductility, the borders between igneous units are often transitional, contrasting to the discordant and sharp contacts they produce against other units, suggestive of intrusion

into a cooler and relatively brittle crust. Pegmatite is observed throughout the map area, from centi- to decimetre scale veins that run concordant with and oblique to the regional schistosity.

The nature of the late plutonic assemblage suggests it may represent a largely heterogeneous collection of in-situ units in which the degree of melting exceeded the critical melt fraction (van der Molen and Paterson 1979) leading to substantial loss in strength and, in turn, a chaotic mixture of various lithologic units. This is supported by the occurrence of numerous rafts and enclaves of sediment apparent in the late plutonic assemblage of the central region, and the occurrence of garnets in some of the granites suggesting hybridisation with the sediments. The opx-granite, however, intrudes as a sill-like body structurally above the central unit, and perhaps the heat for this extensive melting was supplied by this 'hot' opx-granite. The foliation defined by the igneous core units and placed on the map is ostensibly the result of alignment of the K-feldspar megacrysts, likely at the magmatic stage. The megacrysts themselves are undeformed. If the penetrative fabric in the rock had been largely post-magmatic, it would be expected that feldspars augens would be more common.

The nature of the late plutonic units is as follows. The megacrystic granite (Plate 8) is a coarse grained, pink to white weathering, igneous rock similar to the one mapped in the NW GD (Henderson and Schaan 1993). Mineralogically it contains megacrysts of pink microcline, in a quartz, plagioclase, K-feldspar and biotite groundmass, locally containing garnet and rarely pyroxene. In this case, the pyroxene may be magmatic or derived from the melting of mafic material or the psammites. The garnet granite, on the other hand, is a fine to medium grained pink weathering equigranular granite, containing quartz, plagioclase, K-feldspar, biotite, and garnet. The leucogranite is a medium grained, distinctively bright white weathering, felsic igneous rock. Mineralogically it contains quartz, plagioclase, K-feldspar, and biotite, with a flow foliation depicted in the mica. On the eastern flank of the opx-granite ridge, is a conspicuous, 1 - 2 m thick, leucogranite sill (Plate 9). The intrusion facilitates the break-up of a neighbouring

sediment unit into deformed enclaves, and suggests the leucogranite is younger than the metagranitoid and the opx-granite.

The opx-granite is a coarse grained, distinctly orange-brown weathering to dark greasy green when fresh, charnockitic igneous rock. The characteristic colour of this rock, in both cases, is attributed to the presence of microscopic orthopyroxene distributed regularly throughout the matrix. The presence of orthopyroxene testifies to a high temperature of crystallisation. One large sill of opx-granite forms a prominent ridge along the SW shore of Boomerang Lake, at a true thickness of approximately 250 m (Plate 9). Mineralogically it contains quartz, plagioclase, K-feldspar, biotite, pyroxene and sometimes garnet (from sediments), although locally biotite may be absent in hand sample. The rock is generally foliated, interpreted as a magmatic alignment, but sometimes massive and equigranular, or porphyritic in texture.

The pegmatite is a pink, quartz, plagioclase, K-feldspar, and biotite unit, at one location containing macroscopic magnetite crystals (881 - 585), commonly retrograding the country rocks implying that they intruded after the area had cooled down somewhat. The pegmatite is a pervasive unit, observed intruding across all of the FL area, occurring as decimetre to metre scale veins (Plate 10), and sometimes forming caps to ridges. The intrusions of pegmatite are crosscutting, sometimes emanating in orientation from the core, and other times running concordant with the local foliation. In some cases, pegmatites are found within extensional shear zones (Chapter 4).

Plate 3. (854-580) Medium to coarse grained migmatitic paragneiss (metatexite), consisting of rusty brown weathered paleosome and white trondhjemitic peraluminous leucosomes. Garnet is common in hand specimen, cordierite is less common. Notebook is 17 cm long.

Plate 4. (879-587) Medium to coarse grained granitoid gneiss displaying characteristic banding on a decimetre-scale. Notebook is 17 cm long.

Plate 5. (870-609) Medium grained layered mafic granulite with small discontinuous leucosome sweats containing orthopyroxene.

Plate 6. (878-588) Mafic granulite enclave disrupted by a network of sweats, lenses, and veins of melt, containing macroscopic orthopyroxene and to a lesser extent, clinopyroxene.

Plate 7. (878-588) Sweat containing large orthopyroxene and clinopyroxene crystals.

Plate 8. (881-596) Coarse grained, pink to white weathering megacrystic granite. Megacrysts of K-feldspar are aligned syn-kinematically with S_2. Notebook is 17 cm long.

Plate 9. (876-589) 'Orange Mountain' on the southwestern shore of Boomerang Lake. The sill of orange-brown weathering opx-granite forms a prominent ridge. White band across ridge is an intrusion of leucogranite. Bay offers easy dock for float plane.

Plate 10. (888-598) Pink, coarse grained pegmatite intrudes brittle mafic granulite country rock.

3.5 Granulite-Facies Metamorphism

The mineral assemblages of the FL area are diagnostic of high T, medium P granulite-facies metamorphism. The aluminous greywacke is characterised by crd+grt+kfs+melt, probably from the breakdown of bt+sil+qtz with progression from the amphibolite-facies (mineral abbreviations after Kretz 1973). This reaction favours the production of cordierite or garnet at lower and higher pressures respectively, but also depends upon composition, an abundance of cordierite reflecting a Mg-rich protolith, and an abundance of garnet reflecting an Fe-rich protolith (Yardley 1989). Garnet is more prevalent than cordierite in FL sediments, suggesting derivation at high pressures and/or from a protolith with low Mg/Fe ratios. Cordierite rims are also observed mantling garnet, consistent with decompression at high T (Harley 1989).

Ortho- and clinopyroxene occur commonly as macroscopic crystals in the metagranitoids, mafic granulites, psammites and opx-granite, and even when they occur only microscopically in the groundmass, lend a diagnostic dark green hue to the rock when fresh. These rocks are charnockites, a term widened from its original definition that restricted its use to opx-bearing granites (Holland 1900), to include all opx-bearing quartzofeldspathic rocks (Pichamuthu 1969). The metagranitoid assemblage opx+cpx+kfs+pl+qtz+hbl+bt and associated melting is consistent with medium pressure conditions. Orthopyroxene is prevalent over clinopyroxene, pyroxene most likely derived from the breakdown of hornblende and/or biotite. Biotite is still present in varying proportions in all rocks, suggesting that temperatures did not exceed those required for complete dehydration of the granulites. However, plagioclase and quartz leucosome melt are common, especially within the aluminous greywackes, indicating temperatures met those required for the commencement of dehydration melt reactions. According to the evidence, the P-T conditions of metamorphism were high, probably between 750 - 900°C at 6 - 8 kbar (20 - 30 km depth).

3.6 Comparison of Geology of the High-Grade Areas in the SP

The geology of the FL area is similar to the N GD (Henderson and Schaan 1993; Henderson 1994), and the Daran Lake (Pehrsson and Beaumont-Smith 1994; Pehrsson *et al.* 1995) and Snare Lake to Winter Lake regions (Pehrsson and Chacko 1997), located due north of the GD (Fig. 1a). These areas also exhibit similar structural histories (Chapter 4).

These high-grade areas are characterised by:

1. Pronounced high amplitude/short wavelength aeromagnetic anomaly patterns coincident with known exposures of high-grade rocks.
2. Metamorphism in the upper amphibolite- to granulite-facies. Furthermore, Pehrsson and Chacko (1997) report clinopyroxene and hornblende rims on orthopyroxene, and cordierite rims on garnet, consistent with decompression at high T.
3. A distribution of granulite-facies metamorphism known only on a reconnaissance scale. However, from these studies and the current study, the distribution of granulite-facies metamorphism can be delineated as a region encompassing a substantial area to the north and south of Ghost Lake.
4. A temporal-spatial relationship between the granulite-facies high-grade metamorphism and the intrusion of the late plutons.
5. Granitoid gneisses, of granodiorite to monzodiorite composition, that cover a large part of the outcrop area, exhibiting compositional layering and ubiquitous amphibolite to mafic granulite enclaves (composing 10 - 20% of the rock) and constituted of hornblende + clinopyroxene + orthopyroxene + plagioclase.
6. Metasedimentary rocks that predominate over a minor or absent volcanic component, occurring as well-layered migmatitic paragneiss, with 10 - 40% leucosome, to homogeneous diatexite, with dispersed blocks of psammite, signified by the assemblage garnet + cordierite + microcline ± sillimanite ± orthopyroxene.
7. Sheets and dykes of the late plutonic assemblage composed of megacrystic, opx- and leuco-granites, massive to weakly foliated, with abundant sedimentary inclusions.

8. Geology that is thought to represent a deeper-level equivalent of the surrounding lower grade, shallower level rocks.

3.7 Geochemistry

Major- and trace-element analysis was conducted on 21 samples collected from Forked Lake (Table 1; Creaser, pers. comm., 1996). Major oxides were determined by XRF, and the REE and some of the trace elements by ICP-MS (Hooper *et al.* 1993, Knaack *et al.* 1994).

3.7.1 Igneous Rocks

- Metagranitoids

The metagranitoids plot in the calc-alkaline portion of an AFM ($FeO^*+Na_2O+K_2O$) diagram (Fig. 6), have metaluminous to weakly peraluminous compositions with increasing SiO_2 content (Fig. 7; Table 2), and range from tonalites to granodiorites (Fig. 8). The major element oxides are present in the usual way as for many calc-alkaline batholiths, with moderate to high Al_2O_3 contents, relatively low TiO_2 contents, high alkali contents ($Na_2O/K_2O > 1$), and, with the exception of K_2O and Na_2O, decrease approximately linearly relative to increasing SiO_2 (Fig. 9). The SiO_2 can be as low as 49-54% (Table 1), attributed to the accumulation of amphibole and/or plagioclase in some parts of the rock. According to the trace element discrimination plots of Pearce *et al.* (1984), the rocks are representative of volcanic arc and syn-collisional granitoids (Fig. 10a-b). Calc-alkaline rocks with subduction zone signatures do not necessarily reflect a zone of active subduction, and are common in collisional to post-collisional settings also. In these cases, the subduction signature is a reflection of the melting of a source region which was involved in subduction prior to magma generation (Morris and Hooper 1997). Furthermore, the mobility of the large ion lithophile elements (LILE) during granulite-facies may be responsible for some blurring of this signature, primarily in terms of the mobility of Rb in Fig. 10b. The REE patterns for these rocks are steep

with concave up to flat LREE and concave down HREE (Fig. 11a), with La_n/Yb_n of 8.7 to 57.5 produced by a large HREE depletion. Eu anomalies are generally small or absent, with positive Eu/Eu* values of 1.23 to 1.84, and small negative anomalies in the two mafic phases, FL40 and FL2B. Under reducing conditions, Eu^{2+} is less incompatible in plagioclase than the other trivalent REE (substituing for Ca^{2+}), leading to a prominent positive Eu anomaly in plagioclase. Thus, magmas in which plagioclase has separated, result in the a prominent negative Eu anomaly. The highest abundance of REE occur within the most mafic samples and in general decrease with increasing SiO_2 content. The pattern shapes are generally similar over the range of SiO_2, with only a minor crossing of patterns.

- Late Granitoids

The late granitoids plot in the calc-alkaline portion of an AFM diagram (Fig. 6), trending further towards the alkalic apex of the diagram than the metagranitoids, and are peraluminous in composition (Fig. 7, Table 2). The late granitoids are composed of opx-, megacrystic- and leuco-granites. The megacrystic- and leuco-granites are true granites, whereas the opx-granite fall in the range of quartz monzonite to granodiorite (Fig. 8). The basic trends of the major element oxides of these rocks is similar to that of the metagranitoids, apart from a tighter range of SiO_2 between 61-76%, the megacrystic- and leuco-granites are more potassic ($Na_2O/K_2O < 1$), and the opx-granite is the most alumina rich unit. When plotted on the trace element discrimination plots of Pearce *et al.* (1984) (Fig. 10a-b), the late granitoids lie within the same field as the metagranitoids, as that of volcanic arc and syn-collisional granites.

The REE patterns for these rocks have steep concave down to flat LREE and HREE, and concave up MREE (Fig. 11c). The La_n/Yb_n ratios vary from 7 to 102 as a result of variable LREE enrichment, and have petrological significance. The leucogranites are at the high end of the La_n/Yb_n range with ratios of 102 and 77, indicating garnet in their source region, a source similar, perhaps, to the sediments of the

FL area which contain abundant garnet. The opx-granite has La_n/Yb_n ratios of 27 and 63, but these ratios are still considerably higher than typical granites which have similar ratios to the megacrystic granite (La_n/Yb_n = 7). These high values indicate a garnet residue in the source area. The weakly peraluminous nature of the opx-granite suggests a meta-igneous source rock of mafic or intermediate composition. Garnet does not develop in such bulk compositions except at much deeper crustal levels (Green 1982). This suggests a deeper-level, garnet-bearing source region for the opx-granite and a shallow, garnet-free source region for the megacrystic granite. Some of the variation in the REE patterns may be a result of accumulation or fractionation of REE-enriched accessory phases, such as garnet and pyroxene. The megacrystic granite displays a prominent negative Eu anomalies (Eu/Eu^* = 0.26-0.87), and the opx-granite and leucogranite record Eu anomalies ranging from the slightly negative (Eu/Eu^* = 0.87) to the strongly positive (Eu/Eu^* = 3.38), indicating magmas in which plagioclase has fractionated or plagioclase has accumulated, respectively.

- Granitoid Classification

Davis *et al.* (1994) categorise the plutonic rocks of the SP into three distinct groups based on their timing relative to deformation (D_2) and metamorphism in the Contwoyto-Nose Lakes area. Group 1 is interpreted to have intruded synchronously with the YKS volcanic rocks, whereas Group 2 intruded syn- to late-peak deformation and metamorphism, and Group 3 largely post-dates this event. Groups 2 and 3 have U-Pb zircon ages ranging from 2625 to 2595 Ma and 2600 to 2580 Ma, respectively (van Breeman 1992). Davis *et al.* (1994) reports that Sm/Nd isotopes for Group 1 and 2 granitoids are a reflection of differentiation of mantle-derived magmas by assimilation of crustal material and fractional crystallisation, while Group 3 indicate a substantial crustal component. Fig. 12(a-d) displays three spider diagrams plotting the trace element data from Forked Lake with the data set of Davis *et al.* (1994) for the Yamba Suite of Group 3, and the Olga Suite of Group 1.

The Yamba Suite is characterised by biotite granites, weakly peraluminous with typically high contents of K_2O (>4%), often with accessory garnet and have high SiO_2 (generally >68%) and, in some cases, strongly negative Eu anomalies (Fig. 11b). The late plutons of the FL area are comparable to the biotite granites of the Yamba Suite of Group 3. In Figure 12a, a chondrite-normalised spider plot, the two rock groups display similar depletions in Nb and Sr, although the FL rocks are generally relatively depleted in HREE. In Figure 12b, which is normalised to the Peninsular Range batholith (PRB), both groups are depleted in Y relative to PRB, but the Yamba Suite alone displays a depletion of Sr, and the FL rocks alone display a marked depletion in Th in some cases. The disparity in Sr may be accounted for by the mobility of the LILE during granulite-facies metamorphism, and the difference in Th may reflect variations in the degree of fractionation. In this latter case, more fractionated units such as the leucogranite (77% SiO_2), will have higher concentrations of Th than the opx-granite (62% SiO_2), for example. The tonalite unit is also shown on these diagrams as it bears a geochemical similarity to the Yamba Suite, although a preliminary U-Pb age for the unit (Chapter 5) indicates that it is older than the late plutons by some tens of millions of years, more akin to the ages of the Group 2 plutons. The FL metagranitoids, on the other hand, are comparable to the high-Al_2O_3 Olga Group of Group 1. This is consistent with the field associations, which suggest that the metagranitoids are comparable to the gneiss complex of the HD (Fig. 3), from which an age of 2673.3 ±1.4 Ma was attained from a metavolcanic unit (Villeneuve and van Breeman 1994). In Figure 12c, a chondrite-normalised spider plot, the two groups display similar depletions in Nb, and high Ba, and a similar range of HREE. In Figure 12d, which is normalised to the PRB, both groups also display a large depletion in Th compared to the PRB, although the FL rocks are alone depleted in Rb, most likely due to the mobility of the element during granulite-facies metamorphism.

Davis *et al.* (1994) report that the intrusion of the Group 3 plutons was post-deformational. However, the FL late plutons of Group 3 are syn-kinematic with the

deformation (Chapter 4). This difference in the relative timing between intrusion and deformation highlighted by the FL plutons, is consistent with the deeper crust, that remains 'hotter' for a longer period of time than the shallower crust.

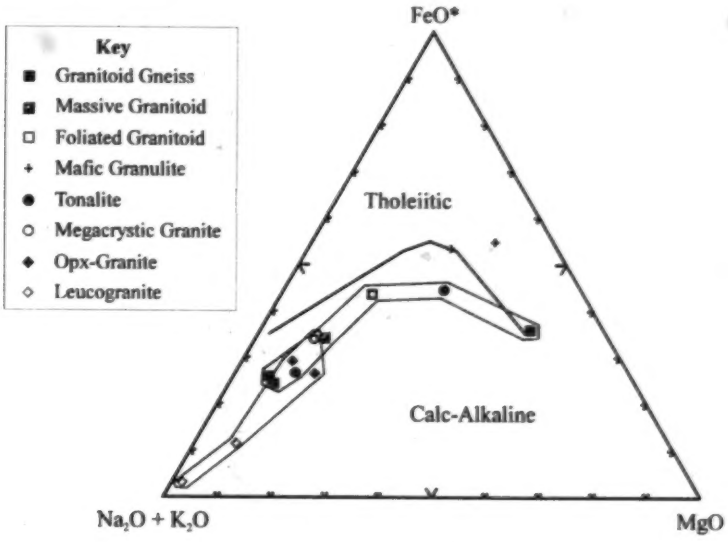

Figure 6. AFM diagram of Irvine and Baragar (1971) plotting the late plutons and metagranitoids, using data from Table 1.

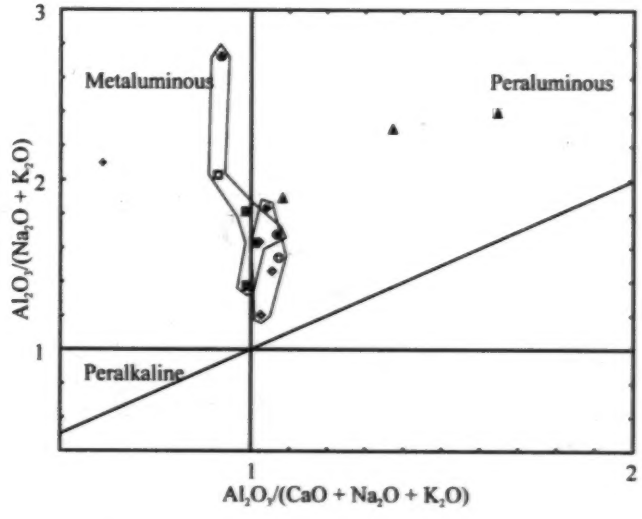

Figure 7. Alumina saturation index (A.S.I.) (Maniar & Piccoli 1989) for FL samples calculated from Table 1. Late plutons and metagranitoids are grouped. Black triangles are sediments, otherwise refer to Fig. 6 key.

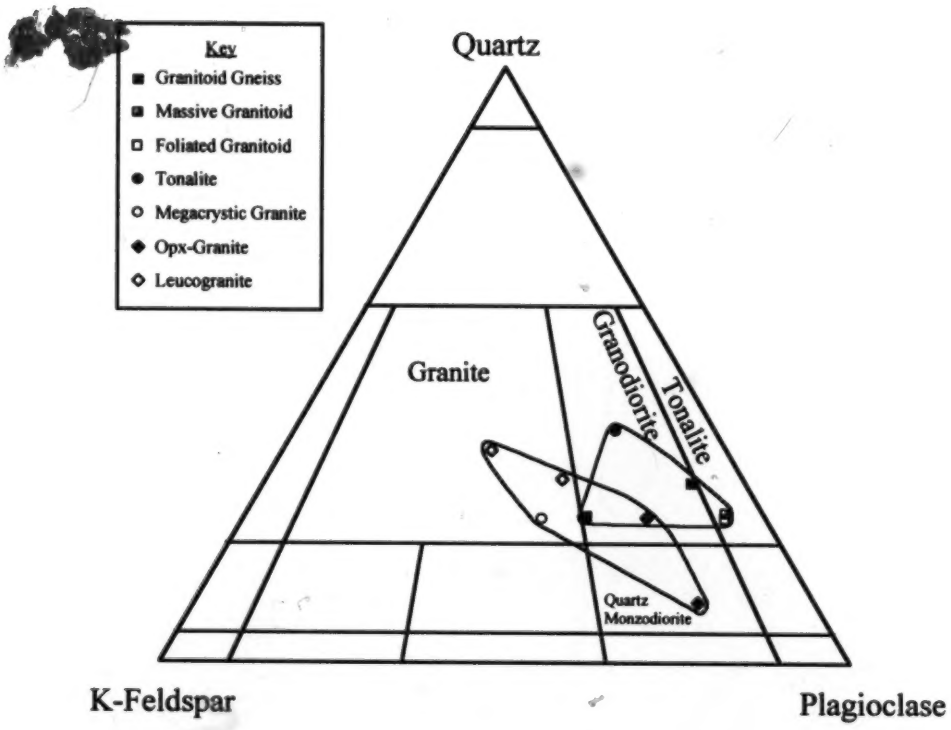

Figure 8. IUGS granitoid classification diagram showing plotted CIPW norms calculated for the Forked Lake metagranitoids and late plutons from XRF oxide values from in Table 1.

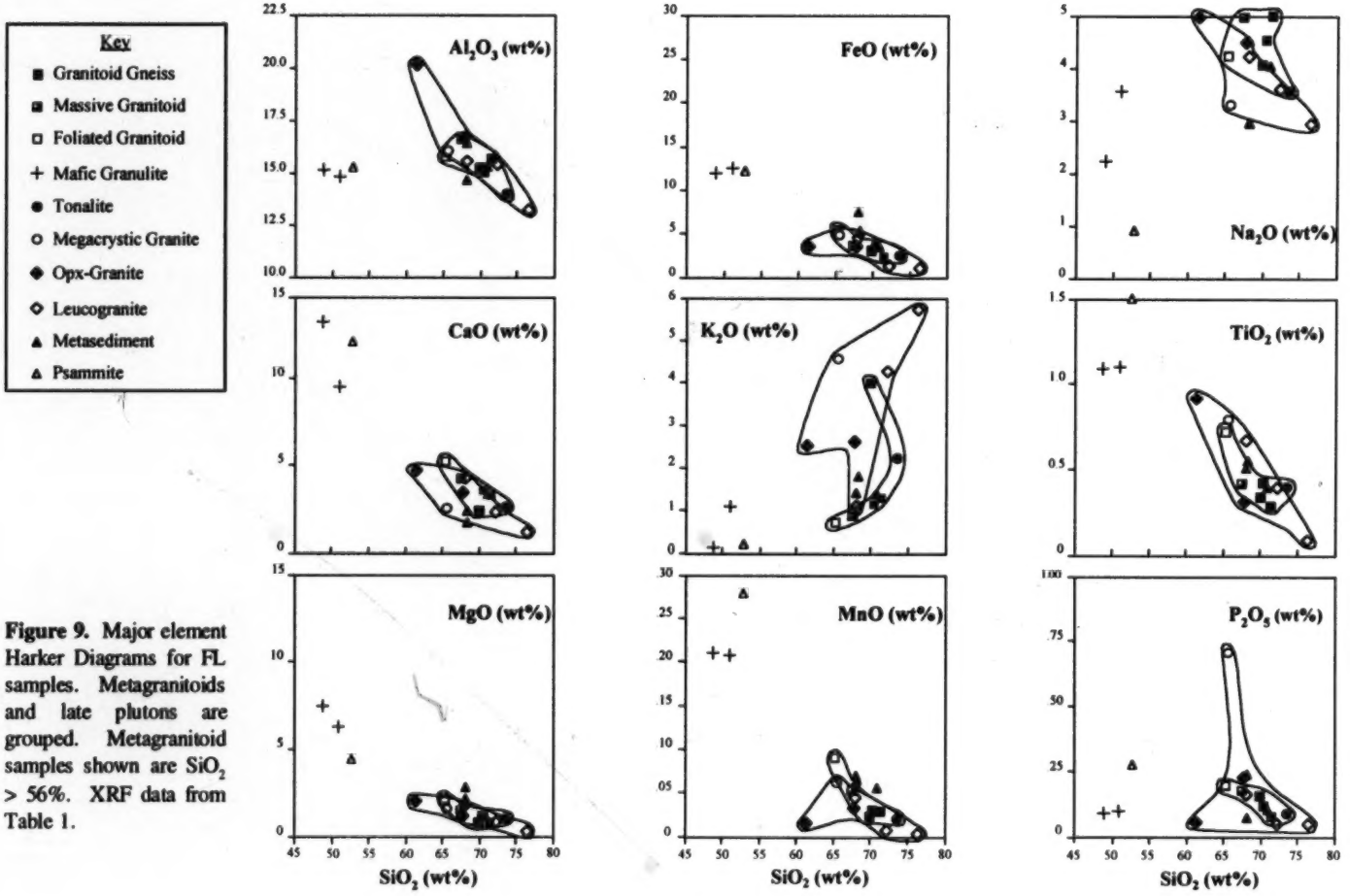

Figure 9. Major element Harker Diagrams for FL samples. Metagranitoids and late plutons are grouped. Metagranitoid samples shown are SiO_2 > 56%. XRF data from Table 1.

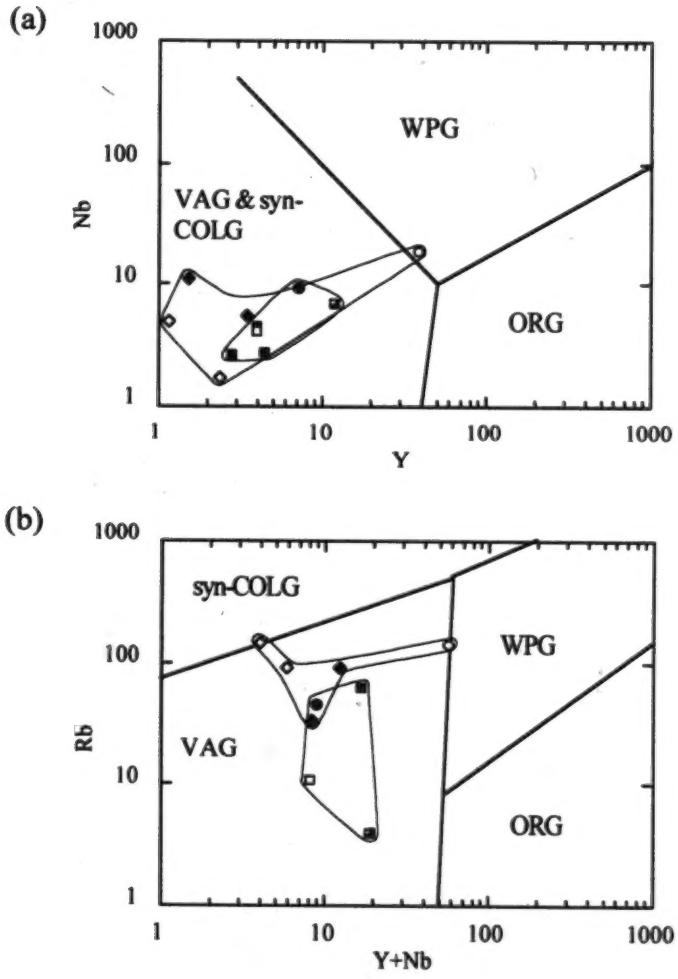

Figure 10. Granitoid trace discrimination diagrams (Pearce *et al.* 1984) for FL metagranitoids and late plutons using data from Table 1. (a) Nb vs. Y; (b) Rb vs. Y + Nb. WPG = within plate granite; VAG = volcanic-arc granite; syn-COLG = syn-collisional granite; ORG = orogenic granite. Metagranitoids: solid square = granitoid gneiss; half-filled square = massive granitoid; empty square = foliated granitoid; solid circle = tonalite. Late plutons: empty circle = megacrystic granite; solid diamond = opx-granite; empty diamond = leucogranite.

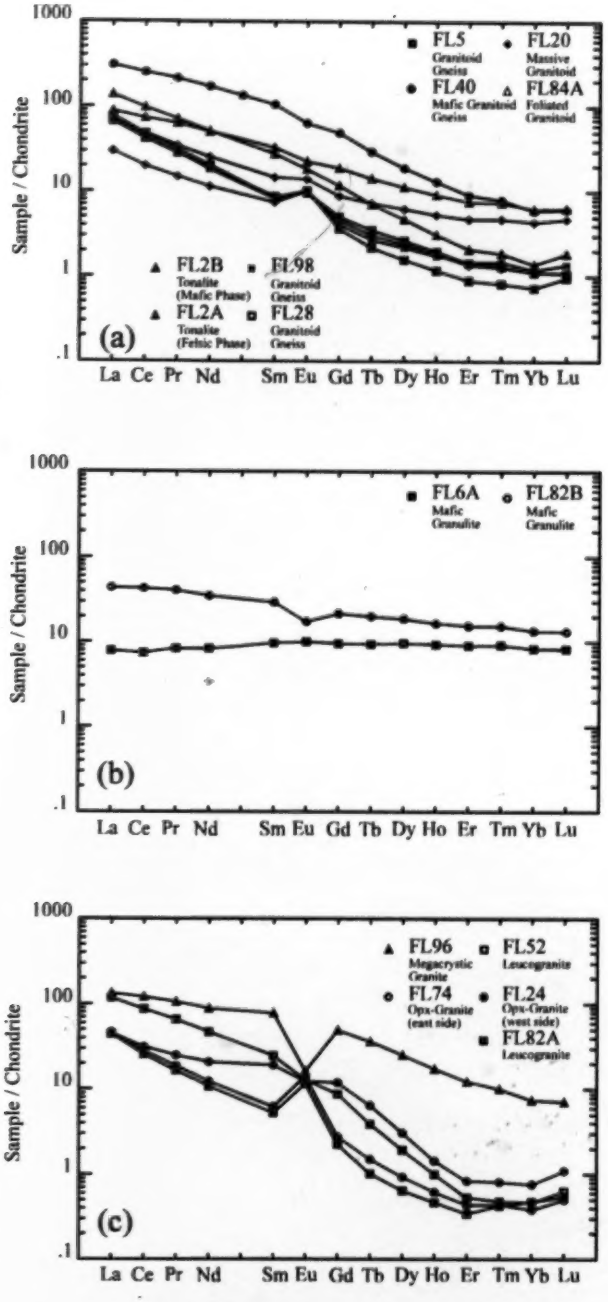

Figure 11. Rare earth element plots for (a) the metagranitoid rocks, (b) the mafic granulites, and (c) the late plutonic rocks. Chondrite normalising values from Taylor and McLennan (1985).

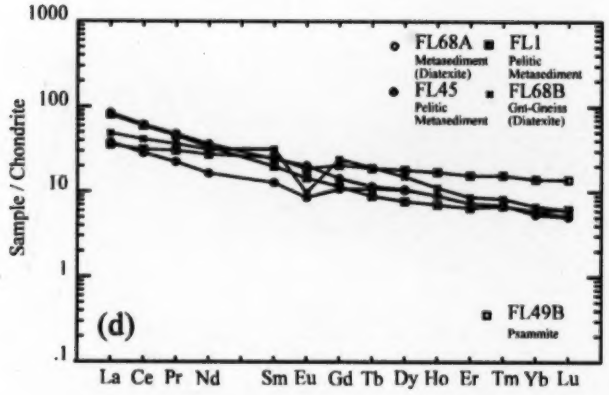

Figure 11. (d) Rare earth element plot for metasediments, using chrondrite normalising values of Taylor andMcLennan (1985).

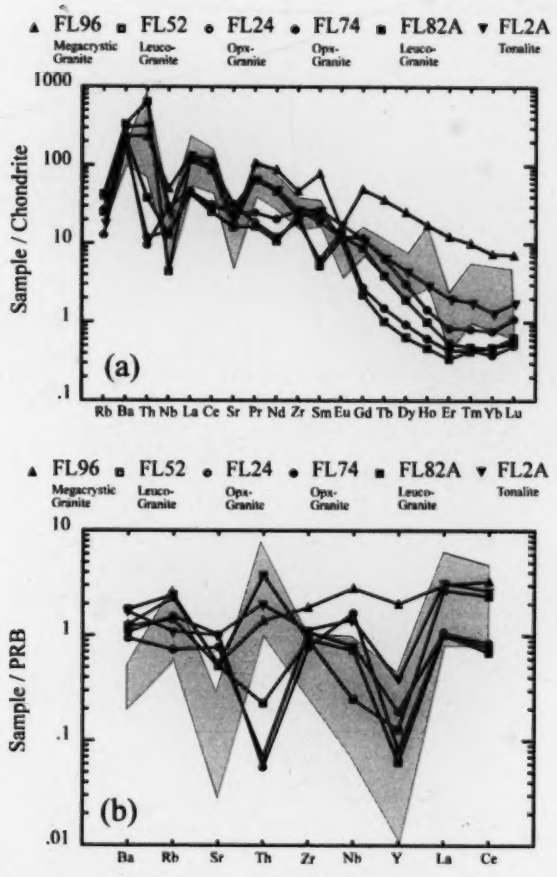

Figure 12 a-b. Chemical composition of the FL late plutons and tonalite. (a) Grey shade is Yamba Suite (Group 3 of Davis *et al.* 1994). (b) Grey shade is Yamba Suite. Diagrams normalised to the average composition of the Peninsular Range batholith (PRB) (65% SiO_2; Silver and Chappell 1988).

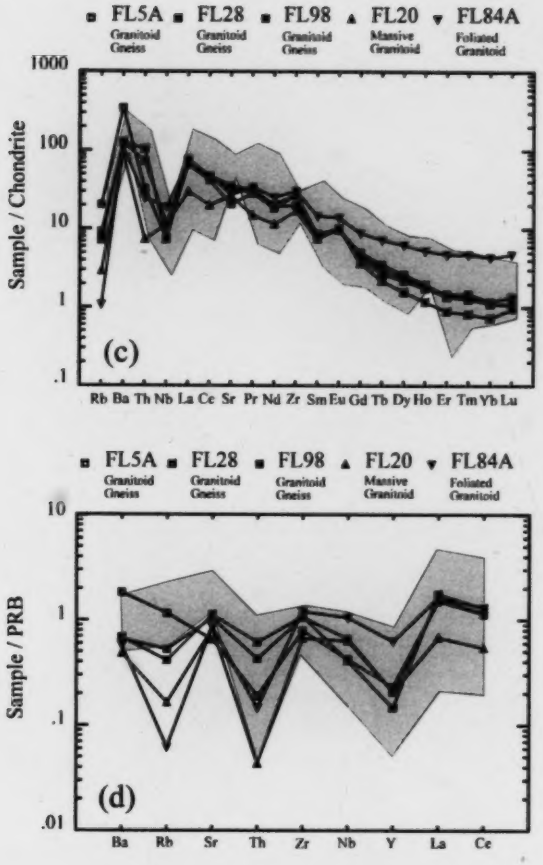

Figure 12 c-d. Chemical composition of the FL metagranitoids. (a) Grey shade is Olga Suite (Group 1 of Davis *et al.* 1994). (b) Grey shade is Olga Suite.
Diagrams normalised to the average composition of the Peninsular Range batholith (PRB) (65% SiO_2; Silver and Chappell 1988).

	Metasediment				Tonalite		Granitoid Gneiss	
	FL1	FL45A	FL49B	FL68A	FL2A	FL2B	FL5A	FL28
	Graywacke	Graywacke	Psammite	Gnt-Gneiss	Felsic phase	Mafic phase		
Grid Ref:	854-581	860-607	883-604	875-600	853-582	853-582	871-610	855-580
Majors (%)								
SiO_2	68.16	68.07	52.70	70.84	73.60	54.92	69.89	71.42
Al_2O_3	16.40	14.68	15.30	15.31	13.94	18.44	15.21	15.64
TiO_2	0.66	0.52	1.49	0.39	0.40	0.98	0.34	0.29
FeO*	5.29	7.52	12.20	3.52	2.49	7.97	3.10	2.27
MnO	0.07	0.07	!0.28	0.06	0.02	0.11	0.02	0.03
CaO	1.72	2.38	12.14	3.33	2.61	7.30	2.39	3.23
MgO	2.84	2.15	4.48	1.08	1.04	5.36	0.80	0.78
K_2O	1.82	1.44	0.23	1.35	2.25	1.31	4.02	1.28
Na_2O	2.96	2.93	0.91	4.03	3.57	3.25	4.07	4.99
P_2O_5	0.08	0.24	0.28	0.10	0.09	0.36	0.16	0.08
Trace (ppm); *XRF*								
Ni	64	40	32	8	11	56	8	7
Cr	150	82	139	25	8	126	10	12
Sc	9	12	39	6	10	24	6	4
V	106	75	249	63	41	154	48	32
Zr	137	167	143	124	156	171	110	151
Ga	19	15	20	16	16	24	19	24
Cu	47	48	7	18	11	41	4	15
Zn	85	59	!236	46	45	106	38	40
Trace (ppm); *ICPMS*								
La	29.48	30.81	12.94	13.95	50.40	32.26	24.23	28.05
Ce	56.63	58.42	29.93	27.11	92.88	69.52	39.71	45.34
Pr	6.27	6.51	4.12	3.05	9.75	8.60	3.84	4.29
Nd	23.54	25.83	19.39	11.67	36.21	35.73	13.64	14.38
Sm	4.56	5.54	5.82	2.95	6.33	7.49	2.01	1.94
Eu	1.26	1.76	1.61	0.74	1.57	1.96	0.83	0.88
Gd	3.50	4.36	6.26	3.29	3.58	5.73	1.52	1.10
Tb	0.51	0.67	1.09	0.63	0.41	0.82	0.20	0.13
Dy	2.93	4.06	6.85	3.96	1.78	4.27	1.00	0.60
Ho	0.60	0.76	1.44	0.76	0.26	0.77	0.17	0.10
Er	1.60	1.82	3.87	1.81	0.52	1.87	0.35	0.22
Tm	0.24	0.24	0.55	0.25	0.07	0.26	0.05	0.03
Yb	1.48	1.43	3.45	1.33	0.34	1.53	0.27	0.18
Lu	0.23	0.20	0.53	0.19	0.07	0.24	0.04	0.04
Ba	491.60	416.13	105.28	284.76	1081.74	492.91	1170.76	437.24
Th	6.12	5.86	0.66	2.92	14.20	2.44	1.37	4.42
Nb	6.91	4.53	7.84	7.17	9.46	14.17	2.83	2.73
Y	16.08	21.01	37.16	21.37	7.13	21.31	4.39	2.79
Hf	3.76	3.80	3.89	3.22	4.57	4.10	2.60	3.83
Ta	2.50	0.76	1.68	2.62	3.95	1.81	0.90	2.13
U	1.20	1.19	0.32	0.29	0.88	0.82	0.20	0.18
Pb	14.82	12.54	3.81	10.45	13.85	8.57	12.22	8.19
Rb	59.56	35.02	5.13	43.16	65.52	45.53	69.76	24.74
Cs	1.87	0.56	0.05	0.33	0.81	1.18	0.17	0.21
Sr	288.67	320.55	50.50	262.36	375.40	514.92	244.22	420.97
W	1676.87	15.66	33.73	2011.45	2915.91	817.89	2.54	1728.38

Table 1: Major oxide (wt%) and trace elements (ppm) for the Forked Lake area. Major element and trace element analyses from Ni to Zn conducted by XRF, and other trace elements by ICP-MS, at WSU GeoAnalytical Laboratory. Major elements are normalised on a volatile-free basis, with Fe expressed as FeO*. "!" denotes values >120% highest standard.

	Granitoid Gneiss		Massive Granitoid	Foliated Granitoid	Mafic Granulite	
	FL40 Mafic band 857-615	FL98 856-580	FL20A 867-593	FL84A 902-602	FL6A 870-609	FL82B 876-590
Majors (%)						
SiO_2	49.08	70.36	67.44	65.28	48.94	51.20
Al_2O_3	11.26	15.04	16.62	15.80	15.03	14.71
TiO_2	1.13	0.42	0.42	0.73	1.08	1.09
FeO*	9.03	3.63	3.75	5.51	11.79	12.45
MnO	0.21	0.03	0.05	0.09	0.21	0.21
CaO	12.31	3.58	4.23	5.25	13.15	9.41
MgO	12.66	1.15	1.43	2.15	7.37	6.20
K_2O	1.60	1.15	0.89	0.75	0.12	1.08
Na_2O	1.84	4.53	4.99	4.24	2.22	3.55
P_2O_5	0.88	0.12	0.18	0.20	0.08	0.09
Trace (ppm); *XRF*						
Ni	167	14	18	30	121	87
Cr	611	12	15	28	254	224
Sc	29	7	12	15	42	38
V	164	54	41	97	280	268
Zr	217	147	93	168	54	75
Ga	15	18	22	20	15	24
Cu	227	4	17	35	94	19
Zn	148	53	75	91	84	154
Trace (ppm); *ICPMS*						
La	112.18	24.91	10.91	26.37	2.88	16.05
Ce	240.40	41.36	19.04	45.69	7.08	40.71
Pr	29.23	3.92	2.04	4.70	1.14	5.56
Nd	121.93	12.85	8.09	17.88	5.91	24.72
Sm	24.34	1.88	1.71	3.37	2.24	6.77
Eu	5.46	0.85	0.87	1.21	0.87	1.50
Gd	14.92	1.24	1.39	2.69	2.94	6.58
Tb	1.68	0.16	0.18	0.42	0.55	1.16
Dy	7.18	0.83	0.91	2.37	3.67	7.15
Ho	1.11	0.15	0.15	0.45	0.79	1.41
Er	2.25	0.37	0.34	1.17	2.25	3.84
Tm	0.28	0.05	0.04	0.17	0.33	0.55
Yb	1.46	0.29	0.28	1.08	2.07	3.33
Lu	0.23	0.05	0.04	0.18	0.31	0.50
Ba	971.32	426.55	308.10	369.71	26.16	219.39
Th	4.30	3.09	0.31	1.05	0.07	0.29
Nb	17.09	4.44	4.23	7.05	2.61	7.66
Y	29.10	3.94	3.90	11.90	20.83	38.73
Hf	5.19	3.07	1.86	3.84	1.43	2.18
Ta	1.09	1.43	0.99	1.67	0.62	1.38
U	2.53	0.17	0.20	0.18	0.02	0.31
Pb	4.02	6.63	7.55	4.05	0.69	4.66
Rb	83.51	31.58	9.89	3.73	2.41	13.04
Cs	1.49	0.43	0.31	0.03	0.04	0.13
Sr	449.19	391.99	309.53	321.66	109.18	167.66
W	340.85	3.67	5.44	11.51	40.49	42.88

Table 1 (continued)

	Opx-Granite		Leucogranite		Megacrystic Granite	BIF
	FL24 (west side)	FL74 (east side)	FL52	FL82A	FL96	FL10A
	876-590	903-594	887-599	876-590	881-596	879-601
Majors (%)						
SiO_2	68.00	61.61	76.62	72.40	65.58	52.74
Al_2O_3	16.60	20.05	13.17	15.29	16.03	12.25
TiO_2	0.30	0.91	0.08	0.39	0.80	0.55
FeO*	3.35	3.38	0.29	1.11	4.87	28.14
MnO	0.03	0.01	0.00	0.01	0.06	0.10
CaO	3.36	4.60	1.05	2.22	2.50	2.54
MgO	1.07	1.89	0.17	0.75	1.57	3.51
K_2O	2.59	2.50	5.67	4.24	4.58	0.06
Na_2O	4.47	4.99	2.92	3.57	3.31	0.05
P_2O_5	0.22	0.05	0.05	0.04	0.71	0.06
Trace (ppm); *XRF*						
Ni	6	20	5	11	18	16
Cr	0	27	9	7	33	124
Sc	10	4	3	5	13	16
V	40	87	8	25	76	90
Zr	149	107	126	126	257	85
Ga	21	29	17	20	22	12
Cu	11	18	12	5	13	6
Zn	85	84	23	32	76	58
Trace (ppm); *ICPMS*						
La	16.81	17.00	43.06	16.18	48.79	19.74
Ce	29.77	26.83	83.30	24.28	114.70	37.10
Pr	3.39	2.56	9.02	2.27	14.52	4.12
Nd	14.62	8.63	33.13	7.58	62.66	17.18
Sm	4.39	1.43	5.67	1.21	18.00	4.05
Eu	1.06	1.23	1.11	1.00	1.41	0.89
Gd	3.60	0.84	2.67	0.68	14.97	3.34
Tb	0.37	0.09	0.23	0.06	2.09	0.48
Dy	1.16	0.35	0.73	0.24	9.53	2.84
Ho	0.12	0.05	0.09	0.04	1.47	0.56
Er	0.21	0.11	0.13	0.08	3.04	1.50
Tm	0.03	0.02	0.02	0.02	0.36	0.21
Yb	0.19	0.09	0.11	0.12	1.83	1.36
Lu	0.04	0.02	0.02	0.02	0.27	0.20
Ba	600.41	689.18	1132.82	779.55	806.44	9.97
Th	0.51	0.40	27.15	1.63	9.96	3.91
Nb	5.33	10.96	1.65	4.82	18.82	4.23
Y	3.58	1.54	2.41	1.19	38.00	15.26
Hf	4.15	2.57	3.88	2.89	6.93	2.23
Ta	2.30	1.50	2.69	1.00	2.60	0.82
U	0.76	0.23	0.96	0.60	1.39	1.66
Pb	14.11	12.56	38.04	20.92	58.33	9.56
Rb	43.81	91.48	146.30	85.72	137.47	3.28
Cs	0.17	0.73	0.23	0.51	0.60	0.64
Sr	288.49	380.76	200.33	191.81	199.03	6.62
W	1605.63	973.73	2216.32	1.09	12.57	15.01

Table 1 (continued). Abbreviations: opx = orthopyroxene; mega- = megacrystic; BIF = Banded Iron Formation.

Sample	Lithology	A.S.I.	C.S.I.	Mg Number	Rb/Sr
FL1	Graywacke	1.65	2.40	65.07	0.21
FL45A	Graywacke	1.37	2.30	77.80	0.11
FL49B	Psammite	0.64	8.77	73.14	0.10
FL68A	Garnet Gneiss	1.08	1.89	76.52	0.16
FL2A	Tonalite	1.07	1.68	70.54	0.17
FL2B	Tonalite	0.92	2.73	59.79	0.09
FL5A	Granitoid Gneiss	0.99	1.38	79.53	0.29
FL28	Granitoid Gneiss	1.01	1.63	74.43	0.06
FL40	Granitoid Gneiss	0.41	2.37	41.63	0.19
FL98	Granitoid Gneiss	1.12	1.83	75.95	0.08
FL20A	Massive Granitoid	0.99	1.81	72.37	0.03
FL84A	Foliated Granitoid	0.91	2.03	71.98	0.01
FL6A	Mafic Granulite	0.54	3.98	61.53	0.02
FL82B	Mafic Granulite	0.61	2.10	66.74	0.08
FL24	Opx-Granite	1.02	1.63	75.79	0.15
FL74	Opx-Granite	1.04	1.84	64.14	0.24
FL52	Leucogranite	1.02	1.20	63.04	0.73
FL82A	Leucogranite	1.05	1.46	59.78	0.45
FL96	Megacrystic Granite	1.07	1.54	75.63	0.69
FL10A	BIF	2.57	80.37	88.91	0.50

Table 2: Alumina saturation index (A.S.I.) ($Al_2O_3/CaO+Na_2O+K_2O$) and calcic saturation index (C.S.I.) (Al_2O_3/Na_2O+K_2O) (Shand 1947). Also shown for reference is the Mg number (100*FeO/[FeO+MgO]) and Rb/Sr ratios for the Forked Lake rocks. Sample locations shown in Appendix A.

- Mafic Granulite

The Ti/100-Zr-Y (Fig. 13a) and Ti-Zr (Fig. 13b) diagrams provide well defined discrimination for altered or metamorphosed basalt samples (Pearce and Cann 1973). The Ti/100-Zr-Y diagram effectively discriminates "within-plate" basalts (continental and oceanic) from other basalt types; the FL samples do not plot as within-plate basalts (Fig. 13a). The Ti-Zr diagram further constrains the basalt type to either low-K tholeiite or ocean floor basalt (Fig. 13b). The Ti/V ratio can be used as a tectonic discriminant (Shervais 1983), however, the Ti/V ratio for the two FL rocks is 23.1 (FL6A) and 24.4 (FL82B), similar to both calc-alkaline basalts (~20) and the upper range of arc-related basalts. Comparison of the FL rocks trace data to a larger array of elements is made by a multi-element diagram normalising to n-MORB (Fig. 13c). Basalts from various tectonic settings have well-defined patterns on these diagrams, and the FL samples show a similarity to the oceanic-arc tholeiite (Pearce *et al.* 1995), although it lacks a similar depletion in Nb (see below). This interpretation is in accord with the Th/Yb and Zr/Y discriminants of Pearce (1983). The FL6A and FL82B have Th/Yb ratios of 0.03 and 0.09 and Zr/Y ratios of ratios of 2.59 and 1.94, respectively, consistent with tholeiitic-arc and oceanic-arc environments (Th/Yb < 0.3; Zr/Y = 0.5 - 3). Furthermore, both mafic granulites plot in the tholeiitic portion of the AFM diagram (Fig. 6), and the REE plots are flat (Fig. 11b), with La_n/Yb_n of 0.94 to 3.25, as a reflection of large HREE enrichment (from pyroxene fractionation), consistent with island-arc basalts. A pronounced Nb depletion is a distinctive geochemical feature of both calc-alkaline and tholeiitic oceanic-arc basalts (Fig. 13c). The absence of a Nb depletion in the FL samples may be due to Nb contamination from the carbide mill during sample crushing. The above geochemical signatures support the possibility that the FL samples were originally tholeiitic oceanic-arc basalts, although firm evidence towards the nature of their tectonic setting may only come from additional work.

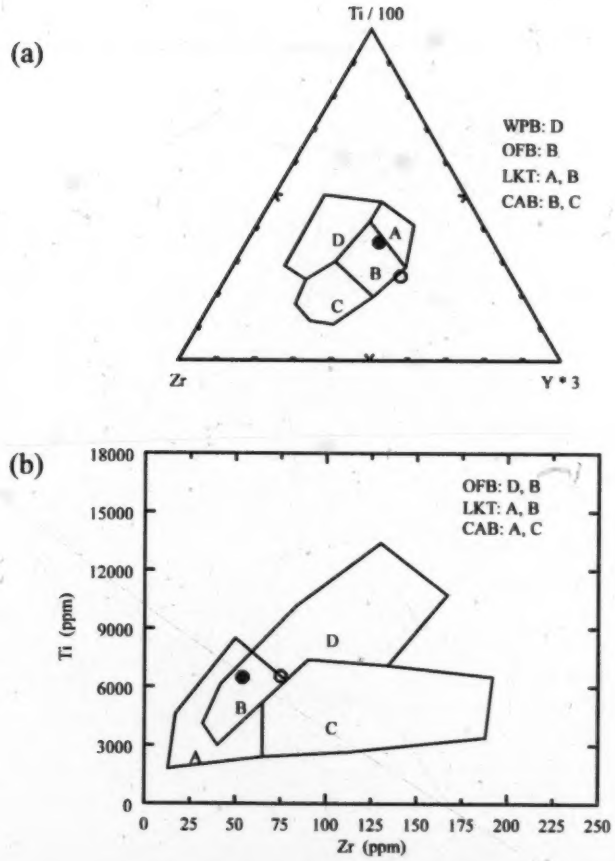

Figure 13 a-b. Trace element differentiation plots for basalt tectonic setting (Pearce and Cann 1973). (a) Ti/100+Zr+Y*3; (b) Ti vs. Zr. See text for discussion. WPB = within plate basalt; OFB = ocean floor basalt; LKT = low-K tholeiite; CAB= calc-alkaline basalt. Solid circle is maif c granulite FL6A, empty circle is mafic granulite FL82B.

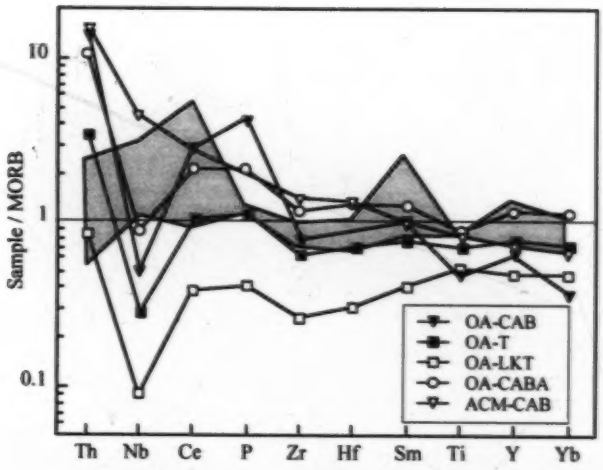

Figure 13c. Incompatible element diagram for immobile trace elements normalised to n-MORB (normalising values from Pearce *et al.* 1995), showing FL samples as shaded zone, as well as respresentative data for basalt types from known tectonic settings (from Creaser *et al.* 1997; Fig. 5). OA-CAB is oceanic arc calc-alkaline basalt, New Hebrides (Gorton 1977; sample 697, 49.4% SiO_2 and 9.4% MgO). OA-T is oceanic arc tholeiite, South Sandwich Islands (Pearce *et al.* 1995; sample SSW 1-1, 49.9% SiO_2 and 6.7% MgO). OA-LKT is oceanic arc low-K tholeiite, South Sandwich Islands (Pearce *et al.* 1995, sample SSC34-2, 50.4% SiO_2, 6.3% MgO). OA-CABA is oceanic arc calc-alklaine basaltic-andesite, South Sandwich Islands (Pearce *et al.* 1995, sample SST 5-1, 55.7% SiO_2 and 3.6% MgO). ACM-CAB is active continental margin calc-alkaline basalt, Turkey (Peccerillo and Taylor 1976, sample T69-21, 52.3% SiO_2 and 8.11% MgO). Shaded area defines area between the two FL mafic granulites (lower line is FL6A; upper line is FL82B). FL mafic granulites most closely resemble oceanic arc-tholeiite (see text for discussion).

3.7.2 Sedimentary Rocks

The aluminous greywacke are strongly peraluminous, and compositionally similar to the Burwash and Walsh Formation greywackes of the YKS and are thus considered to represent their deep level equivalents (Table 3). The greywackes have low Al/Na (<6) compared to other sandstones as indicative of chemical immaturity and derivation from an unweathered source, interpreted to have a mixed felsic-mafic volcanic and granitic source (Taylor and McLennan 1985). The psammites, on the other hand, contrast to the greywacke and mudstone and are enriched in FeO* and CaO, and less $Si0_2$ the greywackes. The high Al/Na of the psammites suggests derivation from a recycled sedimentary source or highly weathered granitic provenance. The REE pattern of the greywackes (Fig. 11d) is shallow sloping with La_n/Yb_n of 8.4 to 10.5, and also lacking a Eu depletion as is characteristic of Archean greywackes. The REE pattern of the psammites is much flatter, however, with HREE enrichment.

	FL1 Greywacke	FL45 Greywacke	Burwash Greywacke	Walsh Formation	FL49 Psammite	Burwash Mudstone
SiO_2	68.16	68.07	68.10	67.79	52.70	56.20
Al_2O_3	16.40	14.68	15.70	15.44	15.30	21.60
TiO_2	0.66	0.52	0.70	0.56	1.49	1.00
FeO*	5.29	7.52	5.30	5.94	12.20	8.60
CaO	1.72	2.38	1.80	1.90	12.14	1.30
MgO	2.84	2.15	2.80	2.54	4.48	5.00
K_2O	1.82	1.44	2.00	1.40	0.23	3.70
Na_2O	2.96	2.93	3.20	4.26	0.91	2.30
K/N	0.61	0.49	0.63	0.25	0.25	1.61
Fe+Mg	8.13	9.67	8.10	8.48	16.68	13.60
Al/Na	5.54	5.01	4.91	3.62	16.81	9.39

Table 3. Forked Lake and Burwash/Walsh Formation sediment major element oxides, and calculated K/N, Fe+Mg and Al/Na values. Burwash/Walsh data from Taylor and McLennan (1985).

3.7.3 Nd Isotopic Data

Nine samples were selected for Sm-Nd isotopic analysis (Table 4), and the data were collected by Creaser using the analytical method outlined in Creaser *et al.* (1997). Initial $^{143}Nd/^{144}Nd$ ratios were calculated using inferred ages of 2590 Ma for the late granitoids, and an age of 2650 Ma for the sediments and metagranitoids. Initial εNd values (εNd_T) were calculated using CHUR reference values of $^{143}Nd/^{144}Nd$ of 0.513163 and $^{147}Sm/^{144}Nd$ of 0.2138. The εNd values are presented in Fig. 14, including for reference the depleted mantle (DM) evolution line of Goldstein *et al.* (1984). The T_{DM} values were calculated by projecting the initial $^{143}Nd/^{144}Nd$ of a sample, along an evolution line determined by the $^{147}Sm/^{144}Nd$ ratio, to intersect DM. The results (Fig. 14; Table 4) are as follows: the late granitoids εNd_T = -0.5 to -0.1 at 2590 Ma, and T_{DM} = 2.89 - 2.91; the metagranitoids εNd_T = -1.4 to 1.3, and T_{DM} = 2.79-3.03; and the sediments εNd_T = -3.0 to -0.2 at 2650 Ma, a T_{DM} = 3.21.

These values are consistent with analyses from the western SP by Davis and Hegner (1992), who, in a regional study of the geochemical characteristics of granitoids of similar age groupings across the province, observed a striking dichotomy in the nature of the underlying crust, reflecting different ages of crustal protoliths in the opposing eastern and western portions of the craton (Fig. 14b). This observation is consistent with the restriction of pre-YKS inliers of Mid to Early Archean age to the western SP (Fig. 1b). Granitoids from the western SP, give rise to εNd_T ranging from +2.7 to -5.3, indicating the involvement, to some extent, of a significantly older and more isotopically evolved crustal component, whereas granitoids from the eastern SP, give positive rise to εNd_T ranging from +0.6 to +3.6, indicating the involvement of a relatively juvenile crustal component. Although the FL samples agree with the given range for the western SP, they are somewhat transitional with those values reported for the eastern SP (Fig. 14a). εNd_T values from sedimentary rocks are considered to reflect the isotopic composition of the sedimentary source or provenance area. A single εNd_T value of -3.0 for a FL sediment is slightly lower than a single analysis reported for the western SP of

εNd_T = -6.4 (Fig. 14a,b), but suggests an older sediment source to that of the eastern and central SP, which display a positive range of εNd_T values of +0.3 to +0.4 (Davis and Hegner 1992).

Recent work by Davis *et al.* (1996) on the Pb isotopic composition of the Late Archean granites has further divided the western SP, advocating that marked differences in isotopic composition reflect a collage of crust of different age, with dominantly older crustal sources to the north (3.9 - 3.2 Ga), a majority of middle-aged sources to the south (ca. 3.2 - 2.9 Ga), and an intervening region of relatively juvenile Late Archean sources around the Ghost Lake region (Robertson and Folinsbee 1974). The rocks of the FL area display εNd_T values indicating assimilation or derivation from rocks with depleted mantle ages between 2.79 and 3.03 Ga (Table 4), consistent with a relatively juvenile underlying crust in the Ghost Lake region as proposed by Davis *et al.* (1996).

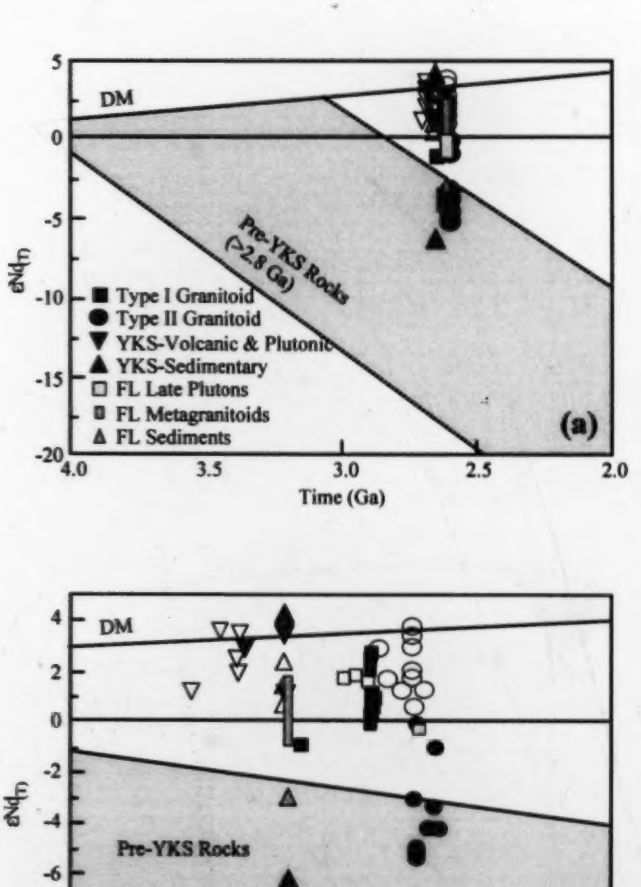

Figure 14. (a) Plot of $\varepsilon Nd_{(T)}$ vs time of crystallisation or deposition of Archean rocks from the western (black symbols) and eastern (white symbols) SP (from Davis and Hegner 1992; Fig. 4), and FL samples (Table 4). Depleted mantle (DM) evolution line from Goldstein *et al.* (1984). The stippled band contains the isotopic evolution paths of pre-2.8 Ga rocks from the western SP (from Davis and Hegner 1992; Fig. 4). **(b)** Detailed view of Nd isotopic data for the principal orogenic period in the SP. Other features as described for Fig. 14a.

Sample Name	Lithology	Nd (ppm)	Sm (ppm)	$^{147}Sm/^{144}Nd$	$^{143}Nd/^{144}Nd$	2σ *10^{-5}	ε $Nd_{(T)}$ (Ma) At 0	2590	2650	T_{DM} (Ga)
FL1	metasediment	21.32	3.98	0.1129	0.511022	0.9	-31.5		-3.0	3.21
FL2A	tonalite	19.16	3.32	0.1047	0.510984	1.0	-32.5		-0.9	3.03
FL2B	tonalite	37.37	7.09	0.1147	0.511278	1.1	-26.5		1.5	2.88
FL24	opx-granite	16.31	4.52	0.1676 *	0.512113	1.3	-10.2	-0.5		3.44 *
FL28	granitoid gneiss	14.07	1.68	0.0721	0.510556	0.8	-40.6		1.9	2.79
FL40	granitoid gneiss	137.11	23.91	0.1054	0.511100	0.8	-30.0		1.1	2.89
FL52	leucogranite	49.93	7.59	0.0919	0.510820	1.5	-35.5	-0.5		2.91
FL68	metasediment	12.07	2.75	0.1380 *	0.511602	1.4	-20.2		-0.2	3.12 *
FL74	opx-granite	8.42	1.31	0.0942	0.510879	0.9	-34.3	-0.1		2.89

Table 4. Sm/Nd isotopic data and $\varepsilon Nd_{(T)}$ values for Forked Lake samples (Creaser, pers. comm., 1997), analytical techniques from Creaser *et al.* (1997). $\varepsilon Nd_{(T)}$ late plutons calculated at 2590 Ma, and the metagranitoids and sediments at 2650 Ma. Depleted mantle (DM) evolution line from Goldstein *et al.* (1984). *Erroneous model age for these samples because of high Sm/Nd ratios.

4. Archean Deformation

4.0 Introduction

The purpose of this chapter is to summarise the Archean structural deformation observed within the Forked Lake area, and to establish these structures in terms of the regional tectonic setting, although this is not intended to be an exhaustive study. The structural analysis of granulite terranes is complicated by the intensity of deformation, the increasing ductility of rocks with melting, the lack of kinematic indicators, and the destruction of prograde microstructures. These factors hinder the resolution and correlation of structures recognised at higher crustal levels. However, despite these problems the FL area represents a relatively pristine window into the peak upper-amphibolite to granulite grade mid-crustal conditions, and as summarised in Fig. 15, the area is characterised by five distinct deformation events (D_1- D_5). These deformation events may be placed in the context of continental thickening (D_1 and D_2) followed by extensional collapse (D_3) of the overthickened zone. Subsequently, the flat lying fabrics of these earlier episodes were tilted to their present pattern by late D_4 - D_5 cross-folding.

Subsequent to the Late Archean deformation, only minor brittle faulting has occurred. Two faults are inferred from a perusal of the topography (Fig. 5, Plate 2), although no evidence for either fault was observed in the field. The Boomerang Lake fault runs along the eastern edge of the area and, if representative of a large displacement, may explain the difficulty in tracing the rim units by air photography across to the eastern side of the dome (Plate 2). The Forked Lake fault strikes NW-SE across the area, and is responsible for the development of the fork of the lake (Fig. 5). Both faults may be associated with the Proterozoic block uplift of the GD (Henderson 1994).

4.1 Deformation of the Forked Lake area (D_1 - D_5)

The first recognisable deformation (D_1) is expressed by a relict schistosity (S_1) observed within the mafic and psammitic enclaves. S_1 is defined by the alignment of

minerals contrary to the regional S_2 schistosity, often contracted within the remnants of decimetre-scale isoclinal fold hinges (Plate 11). The axial planes of these folds are parallel with the regional S_2 schistosity, and are interpreted as F_2 folds. The second period of deformation (D_2) is thus represented by the development of a horizontal regional schistosity (S_2) parallel to the geological contacts, and the rotating of small isoclinal folds (F_2) towards the horizontal. The regional schistosity (S_2) is defined by the alignment of hornblende, pyroxene, and quartz-feldspar aggregates in the metagranitoids, and, also, with the alignment of in-situ pockets of melt containing cordierite and garnet in the sediments. Thus D_2 is interpreted as synchronous with the development of peak-metamorphism.

The observation of a preferred orientation of megacrysts within the late plutonic assemblage is interpreted as a result of intrusion syn-kinematically during D_2. For example, aligned megacrysts in the megacrystic granite (Plate 8), are not deformed into augen shapes as one would expect if such a texture were the product of deformation after intrusion. Conversely, if the intrusion of these units had occurred subsequent to the development of the S_2 regional schistosity, one would expect a random distribution of the megacrysts across the area, like a flow foliation. Instead, the strike-and-dip pattern of the megacrysts conforms to the regional pattern of the S_2 schistosity, that is circular and dome-shaped (Fig. 5), suggesting a deformational control on the formation of this pattern.

The third deformational event (D_3) is characterised by syn- to late-thermal peak extension. Although a switch from contraction to extension, or collision to collapse, is a commonly observed phenomenon from studies of Phanerozoic orogens, the evidence for extensional deformation in the SP has only recently been noted (James and Mortensen 1992). However, Davis *et al.* (1994) report that the intrusive style of post-D_2 granite plutons is consistent with intrusion during extension. At Forked Lake, D_3 extension is expressed by numerous small shear zones (~10 cm wide and 1 m long) that cut almost orthogonal to the S_2 regional schistosity, with observed displacements on a decimetre-scale (Plate 12). When the tilting effects of the doming were removed using a stereonet,

readings from two shear zones on the western side of the map area yielded shear plane orientations of 285/52 NE and 309/54 NE, with top-to-the-north movement. A prolonged period of extension is indicated by pegmatite-absent and pegmatite-intruded shear zones. With the earlier, pegmatite-absent shear zones, leucosomes of melt in the sediments are often seen deforming in a ductile fashion (Plate 12). On the other hand, with the later, pegmatite-intruded shear zones, the sometimes foliated pegmatite exhibits sharp, brittle borders with the country rock, indicating a cooler crust than in the previous case. These younger shear zones may offer a convenient conduit for the transport of pegmatite across the area. Further work on the absolute intrusion age of these pegmatites would constrain the younger age of extension in the FL area. Extension is also manifested in the FL area by the occurrence of rare, brittle structures (Plate 13), also exhibiting top-to-the-north movement.

The final component of the structural history was the tilting of the whole previously horizontal sequence by F_4 - F_5 cross-folding of a Type 1 interference pattern, responsible for the doming of the geology and the circular pattern of strike-and-dip recordings (Fig. 5). The dome structure is supported by stereographic projection of the pole-to-plane of strike-and-dip recordings (Fig. 16), which clearly illustrates the circular spread of the data. In Fig. 16, the number of poles is a reflection of the sampling density, which was concentrated in the NW segment of the area. The cross-folding is arguably post-dating the extension because the latter, as already mentioned, commenced during granulite-facies, whereas the cross-folding does not impose any recognised penetrative fabric on the FL rocks, as would be expected if it had occurred during peak thermal conditions.

D_4-D_5	Type I interference folding: Structural doming
D_3	Syn- to late- extension: Shear zones
D_2	Folding of S_1 Regional schistosity (S_2)
D_1	Schistosity (S_1)

Figure 15. Summary of the structural history of the Forked Lake area.

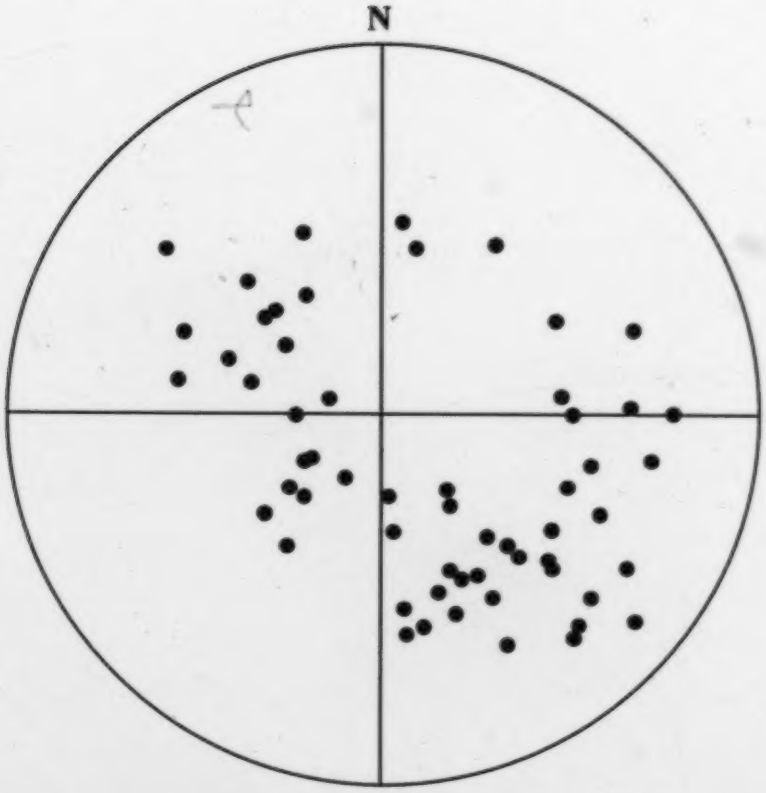

Figure 16. Equal area (Schmidt) stereonet plotting 58 pole-to-plane strike and dip readings of the S_2 schistosity, and syn-kinematic K-feldspar alignments in the late plutonic assemblage. Plotted using SpheriStat for Windows, version 2.1.

Plate 11. (867-593) Isoclinal folds of mafic enclaves in granitoid gneiss. Axial planes of these folds are aligned with regional S_2 schistosity. Notebook is 17 cm long.

Plate 12. (866-598) Shear zone cutting S_2 schistosity in a metasediment, showing ductile deformation of a leucosome band (white). Notebook is 17 cm long.

Plate 13. (876-591) Brittle extensional feature.

4.2 Comparison of Structural Geology of the High-Grade Areas in the SP

The structural character of the FL area is similar to the N GD (Henderson and Schaan 1993; Henderson 1994), and the Daran Lake (Pehrsson and Beaumont-Smith 1994; Pehrsson *et al.* 1995) and Snare Lake to Winter Lake regions (Pehrsson and Chacko 1997), located due north of the GD (Fig. 1a).

The structure of these areas is characterised by:

1. A period of contractional deformation as a result of ongoing shortening and thickening of the continental crust, characterised by the development of a horizontal to shallow-dipping regional planar fabric parallel to geological contacts, developing during peak granulite-facies metamorphism.
2. A switch from contractional to extensional deformation as a result of compressional relaxation, characterised by syn- to late- decimetre-scale shear zones, observed to cut the earlier regional planar fabric. These shears are typically filled by narrow dykes or veinlets of granitoid material, suggesting their activation during peak-thermal conditions. Furthermore, both shearing and granite intrusion as part of a regional extension has been proposed for other parts of the central and southern SP (e.g. Davis *et al.* 1994; Stubley 1994).
3. Late cross-folding trending NW, NE, and E that are responsible for the tilting of the regional planar fabrics from moderate to steep dips.
4. Late uplift of the granulite terrane along proposed Paleoproterozoic oblique normal faults.

5. U-Pb Zircon Geochronology

5.0 Introduction

The U-Pb zircon technique has proven to be a reliable method for obtaining high precision age information on a wide variety of rock-types. The history and modern application of the technique is reviewed by Heaman and Parrish (1991). Zircon ($ZrSiO_4$) is a widely occurring accessory mineral, with a uranium concentration ranging from a hundred to a few thousand ppm. Uranium is incompatible in the major rock-forming minerals (a few ppm or less), but is strongly partitioned into zircon owing to its compatibility for exchanging with Zr (U^{+4} ionic radius = 1.05 A; Zr^{+4} = 0.87 A).

U-Pb zircon geochronology was a suitable choice for this project as it represents a conventional approach towards attaining reliable and quantitative isotopic data, applicable to the unraveling of the igneous and metamorphic relations in the FL area. On account of its high closure temperature (>800°C), zircon acts as a closed system throughout most of the cooling history of a rock, leading to a zircon age that represents a close approximate to the onset of crystallisation (Heaman and Parrish 1991). Furthermore, a high closure temperature closes the zircon isotopic clock to major disturbances during subsequent thermal events.

The relative success of zircon as a geochronometer, however, is primarily due to three factors. To begin with, zircon has a negligible quantity of common Pb (non-radiogenic Pb), owing to the incompatibility of Pb in the crystal structure during crystallisation. Thus, corrections to the calculated U-Pb age arising from common Pb contributions are usually very small. Secondly, zircon crystals that have not recrystallised or suffered radiation damage tend to retain U and radiogenic Pb in their crystal structure because of the very slow diffusion rates of these elements in zircon (Cherniak *et al.* 1997). Therefore, the U-Pb zircon chronometer is much less susceptible to resetting by post-crystallisation geological events than many other minerals and isotopic systems used for geochronology. Finally, the U-Pb system has two unstable

nuclides, ^{238}U (99.28%) and ^{235}U (0.715%), that decay through a series of intermediate daughter products to the stable daughter isotopes of ^{206}Pb and ^{207}Pb, respectively. These two U-Pb geochronometers provide an internal check the degree to which the zircon grains have behaved as closed systems with respect to U and Pb.

5.1 Analytical Procedure

The following section outlines the U-Pb geochronology laboratory procedure conducted on the FL samples at the University of Alberta. The processing of each sample involves the liberation, abrasion, and dissolution of the zircon, followed by the U-Pb isotope chemistry and thermal ionisation mass spectrometry (TIMS). At all times thorough cleaning and clean laboratory conditions were employed to lower the possibility of contamination.

- Liberation, Abrasion, and Dissolution of Zircon

The zircon was first isolated from the host rock by conventional crushing and mineral separation techniques. 5-15 kg of the sample, which was collected free of all visible alteration and weathering and broken up under plastic or on the outcrop, was crushed in a steel-plated jaw crusher. The resulting fragments were ground in a Bico™ disk mill to a fine sand (10 - 300 micron range), and passed over a Wilfrey™ table to obtain a heavy mineral concentrate. The concentrate was sieved over +70 mesh paper to collect the finer grains, then passed in front of a vertically orientated Frantz™ isodynamic separator, removing highly magnetic minerals. Felsic rock samples were further separated by heavy liquids (methylene iodide), producing a mafic sink. The mafic sink was collected and passed over a horizontally orientated Frantz™, with an initial side tilt of 15°. The first zircon fraction was collected as non-magnetic at 1.8 A. Further, cleaner, zircon yields were collected at side tilts of 10° and 5°, and 2° if necessary. Mafic rock samples, on the other hand, after the vertical Frantz™ stage, were run for an initial

Frantz™ with a side tilt of 15° at low amperage to remove the bulk of magnetic minerals before heavy liquid separation and a final pass through the Frantz™.

The liberated zircons were then hand picked under ethanol, in general, selecting transparent zircons from those containing visible inclusions or interior turbidity. The chosen zircons from each fraction were abraded in a holding chamber of an air abrasion device together with 1 - 5 mg of pyrite to act as a polishing agent, to remove fractured or discordant edges. Typical abrasion sessions lasted for 4-6 hours at approximately 4 psi, followed by 1 hour at 3 psi to ensure a smooth polish. The pyrite grains still remaining after abrasion were removed with a dilute HNO_3 (2-4N) wash.

The abraded zircons were then washed and weighed. The zircons were washed once in ethanol, thrice in acetone, then placed in 4N HNO_3 on a hot plate for 1 hour, and finally washed thrice in millipore, and thrice in acetone. After weighing, the zircons were placed in clean Teflon™ bombs (cleaning procedure given in Appendix B), and approximately 20 drops of 48% HF and 2 drops of 7N HNO_3, and a ^{235}U and ^{205}Pb spike were added. The bombs were placed in the oven for dissolution times between 24 and 72 hours at 220°C. Open bombs were then placed on a hot plate until sample evaporation, followed by 8 drops of 3.1N HCl, and resealed and placed back in the oven overnight.

- Isotope Chemistry and TIMS

The AG-1X8 anion exchange resin was held in a mini column suspended over a collection beaker (cleaning procedures given in Appendix B). The resin was conditioned with 3.1N HCl (~15 drops) and the sample loaded to remove impurities such as Zr and Hf, and other REE. In a clean collection beaker, Pb elution commenced with ~15 drops of 6.2N HCl, followed by U elution with ~15 drops of millipore. Two drops of H_3PO_4 (phosphoric acid) were added to the U-Pb solution, and the mixture was evaporated to dryness on a hot plate (~2 - 3 hours).

The samples were loaded onto a rhenium filament in a sample mixture of 3.5 uL H_3PO_4 and 2.0 uL silica gel, and loaded on a VG354 TIMS. Optimum Pb and U data was collected at 1350 - 1450°C and 1450 - 1550°C, respectively.

5.2 U-Pb Geochronology Results

Five geochron samples were processed, one from each of the megacrystic granite (FL96), opx-granite (FL97), and tonalite (FL99), and two from the same outcrop of mafic granulite sampled on consecutive years (FL6A, FL6B); all locations shown in Fig. 5. 25 separate analyses were run in total and the U-Pb data is summarised in Table 5. All data was processed by in-house computer software, except the regression line calculations, which for the megacrystic- and opx-granite used the method of Davis (1982), and for the mafic granulite and tonalite, used the Isoplot program (version 2.91) of Ludwig (1996).

The analytical Pb blank was higher than expected. The typical laboratory blank at the University of Alberta is in the range of 2 - 6 pg. The total Pb blank for the FL zircons ranged from 5 to 40 pg, and some of the megacrystic granite runs approached 300 pg. The total blank for these samples is attributed to a combination of two factors, the laboratory blank and the common Pb originally incorporated into the zircon upon crystallisation, although the former provides the largest of these contributions. The total blank was acceptable for the present work, because of the high concentration of U and Pb in most of the zircons. Only in one sample (FL6B) was the total blank a major hindrance, because these zircons contained extremely low concentrations of U and Pb. All zircons have suffered Pb-loss during the past 500 Ma. This is interpreted to represent the effect of erosion and weathering processes that have brought the SP to its current exposure level. Furthermore, so as to minimise the chances of analysing zircons with prominent Pb-loss even after abrasion, transparent zircons were picked free of inclusion and internal turbidity, especially in the case of some of the larger grains, which were often metamict.

5.2.1 Description of Zircon Populations

- Megacrystic Granite (FL96)

The crystal morphology was indicative of unimpeded growth in a melt, with euhedral and prismatic 2:1 to 3:1 bypyramidal zircons (Plate 14). Some crystals displayed compositional zoning parallel to face, although magmatic adsorption had often rounded edges between faces. No rims or cores were observed. The majority of the zircons were 0.1 - 0.2 mm long, with occasional larger 0.5 mm zircons. A pink and a tan fraction, segregated on the basis of colour, contained both equant and faceted crystals.

- Opx-Granite (FL99)

The crystal morphology was indicative of unimpeded growth in a melt, with euhedral and prismatic 1:1 to 5:1 bipyramidal zircons (Plate 15), with magmatic softening of the edges. Again, no rims or cores were observed. The zircons ranged in length from 0.1 - 0.4 mm, although the shorter, stubby crystals were the most common. A pink and a tan fraction, segregated on the basis of colour, consisted of equant crystals.

- Mafic Granulite (FL6)

Two samples of mafic granulite from *the same outcrop* acquired in consecutive years were processed separately. Zircons liberated from a hand sample of FL6A yielded less than 10 zircons. These zircons were equant and multifaceted, a 'soccer-ball' shape geometry, indicative of restricted growth in a solid medium (Parrish 1990) (Plate 16). The second, larger sample of FL6B, was crudely separated into leucosome-rich and leucosome-poor segments using a rock saw, and were consequently processed individually. Zircon liberated from both samples of FL6B numbered ~20 grains in total, the majority of which were from the leucosome-poor sample (which was 90 - 95% volume of FL6B sample). Most of the zircon grains exhibited similar equant and multifaceted geometries to sample FL6A, although a few were 2:1 to 3:1 oblong-shaped

with round edges, and the odd one or two were prismatic and bladed. All grains were transparent, indicative of a low concentration of U.

- Tonalite (FL99)

The crystal morphology of the tonalite zircons was composed of needle-shaped zircons with 4:1 to 7:1 dimensions, and stubby euhedral and prismatic 2:1 and 3:1 faceted crystals (Plate 17). A pink, tan and needle-shaped fraction were segregated, the former two composed of equant zircons. Core and rim overgrowth relationships were observed and where seen display a small tan core with a pink overgrowth in some cases, and a pink crystal with a tan rim in other cases. This relationship may indicate two periods of tan zircon growth.

5.2.2 Concordia Plots

- Megacrystic Granite (FL96)

The concordia plot for FL96 is shown in Fig. 17. No analysis plotted exactly on concordia, although abrasion generally lowered discordancy. The two fractions, pink and tan, plotted roughly colinear, and although no single regression line could be computed through all of the ellipses, two separate cords were calculated using analyses that were ~1-6% discordant. A 'younger' intercept age of 2598 +6 -4 Ma is calculated from FL96-7, -8, -10, -11, and an 'older' intercept age of 2602 +13 -7 Ma is calculated from samples FL96-3, -6, -9. Runs FL96-1, -2 and -5 were not included in the regression because of a wide error ellipse, a large discordancy (probably resulting from incomplete dissolution of zircon grain), and a high blank, respectively. The older cord is composed predominantly of pink grains (226 - 626 ppm U), and the younger chord predominantly of tan grains (429 - 1359 ppm U). Perhaps this slight difference in ages is the product of two slightly different ages of zircon growth during fractionation, characterised by increasing U content. However, these two ages are the same within error, and thus the former and

more reliable regression line is taken as the best estimate of the crystallisation age of the granite.

- Opx-Granite (FL97)

The concordia plot for FL97 is shown in Fig. 18. No analysis plotted exactly on concordia, although two analyses from each fraction (pink and tan) are colinear and between ~2-10% discordant along a single regression line with an upper intercept of 2589 +3 -2 Ma. The tan fraction exhibits a higher U concentration (562 - 649 ppm) than the pink (384 - 477 ppm).

- Mafic Granulite (FL6)

The concordia plot for FL6 is shown in Fig 19. Five analyses are plotted on the concordia diagram, two from FL6A (FL6A-1, -2), and three from FL6B (FL6B-3, -4, -5). Correlation between the zircons of the two samples was not possible, apart perhaps from FL6B-5, which despite its large error ellipse, lies in line with the FL6A regression line (Fig. 19). The position of this sample above concordia is thought to be a result of incomplete dissolution of the zircon during processing. Although the outcrop from which the FL6 samples were taken from appeared homogeneous, there is a marked difference in the geochemistry of the two samples. The zircons from FL6A have low U (~80 - 100 ppm) and Pb (~50 ppm) concentration, whereas the zircons from FL6B have extremely low concentrations (~5 - 16 ppm U; 3 - 9 ppm Pb). The difference in geochemistry between these samples is also reflected in the Th/U ratios, with a Th/U range of 0.387 - 0.490 for FL6A and 0.170 - 0.245 for FL6B.

The two FL6A zircons fit a regression line with an upper intercept of 2592 ±5 Ma, at an error correlation of 0.99. However, the lower intercept of this regression line was forced through the origin, and, with only three points used in the construction of this line, the error value may be much larger than that quoted (Ludwig 1996). Analysis FL6B-5 was avoided for this calculation because its wide error ellipse inhibits the use of this

analysis for the improvement of the regression line. The two FL6B zircons, on the other hand, fall to the left of the regression line. FL6B-4 lies off the concordia with a $^{207}Pb/^{206}Pb$ age of 2562.5 Ma and FL6B-3 lies transitional with the zircons of FL6A, both with relatively larger error ellipses than the FL6A zircons.

The mafic granulite was the biggest challenge for geochronology, with low zircon yields and low to extremely low uranium content. In this case very low analytical blanks are essential for precision. Analytical blanks in my runs were not low enough for the successful constraining of the FL6B zircons, precluding the acquisition of any further analyses in the current study.

- *Tonalite (FL99)*

The concordia plot for FL99 is shown in Fig. 20. Two independent regression lines have been calculated for this sample. The two zircons analyses, FL99-1 and FL99-2, fall onto a regression line with an upper intercept of 2639 ±6 Ma with a lower intercept of 851 ±84 Ma, calculated at an error correlation of 0.99. The error of the upper intercept cannot be considered as a realistic true error, as only two points were used for the construction of this line, and the true error must be much larger. A second cord is calculated using analyses FL99-1, -2, and -5, with an upper intercept of 2601 ±112 Ma and a lower intercept of -8 ±217 Ma. Analysis FL99-5 is not shown in Fig. 20, but lies 74% discordant, and is responsible for the large error in this age. Thus the former age is considered as the most appropriate at this stage, although it is obvious from the data that further analysis is required to place a zircon closer to concordia in order resolve the problem of large age errors. The two analyses from the tan fraction have much younger $^{207}Pb/^{206}Pb$ ages of 2582.8 and 2574.1 Ma, and are much higher U (663 - 723 ppm) than the pink fraction (211 - 416 ppm), and may represent a younger zircon growth, as discussed below.

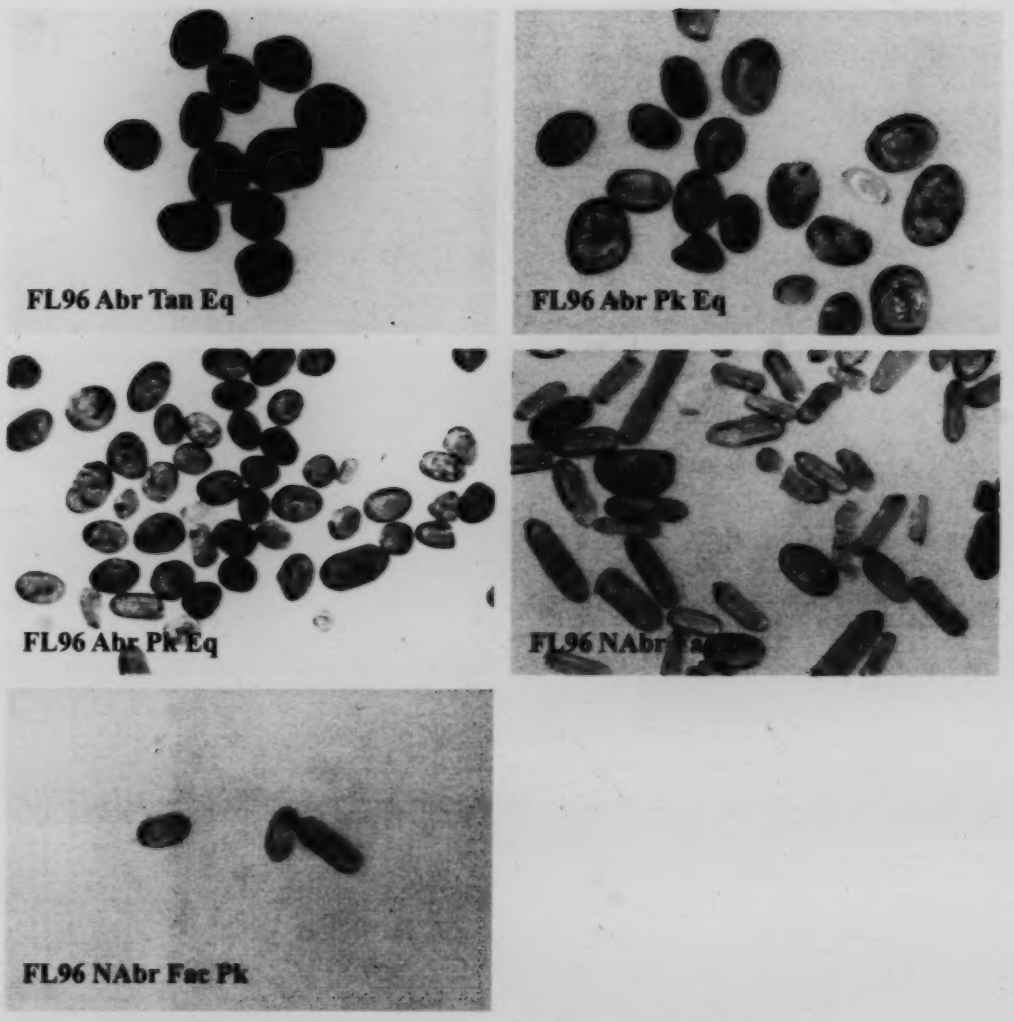

Plate 14. Megacrystic granite zircon fractions. Magnification x100. Abr = abraded; NAbr = non-abraded; Tan = brown; Pk = pink; Eq = equant; Fac = faceted.

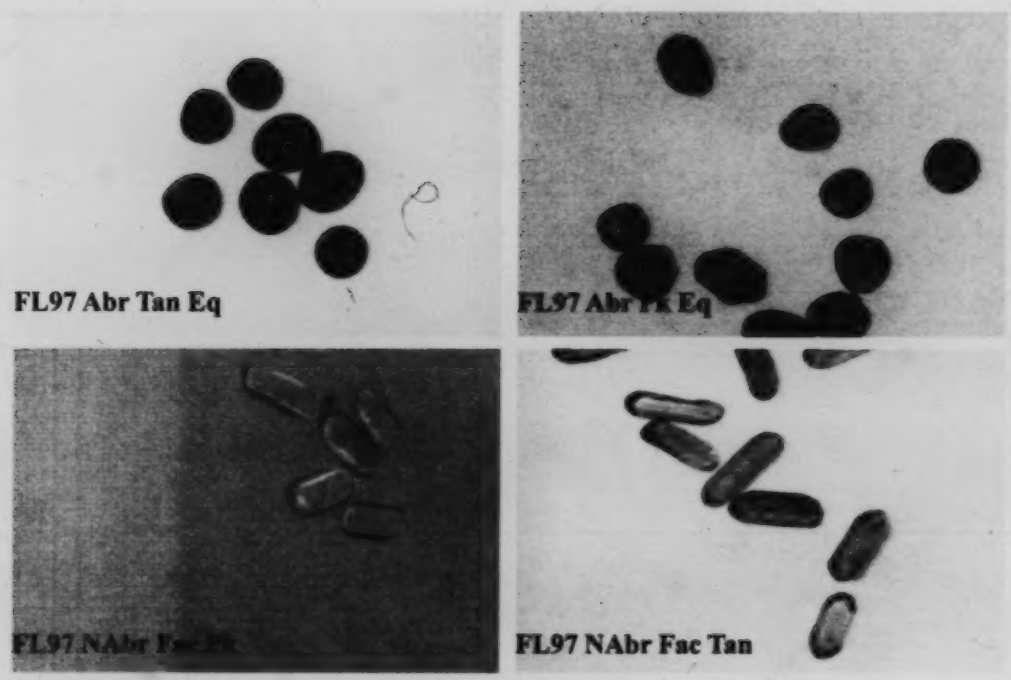

Plate 15. Opx-granite zircon fractions. Magnification x100. Abr = abraded; Tan = brown; Pk = pink; Eq = equant; NAbr = non-abraded; Fac = faceted.

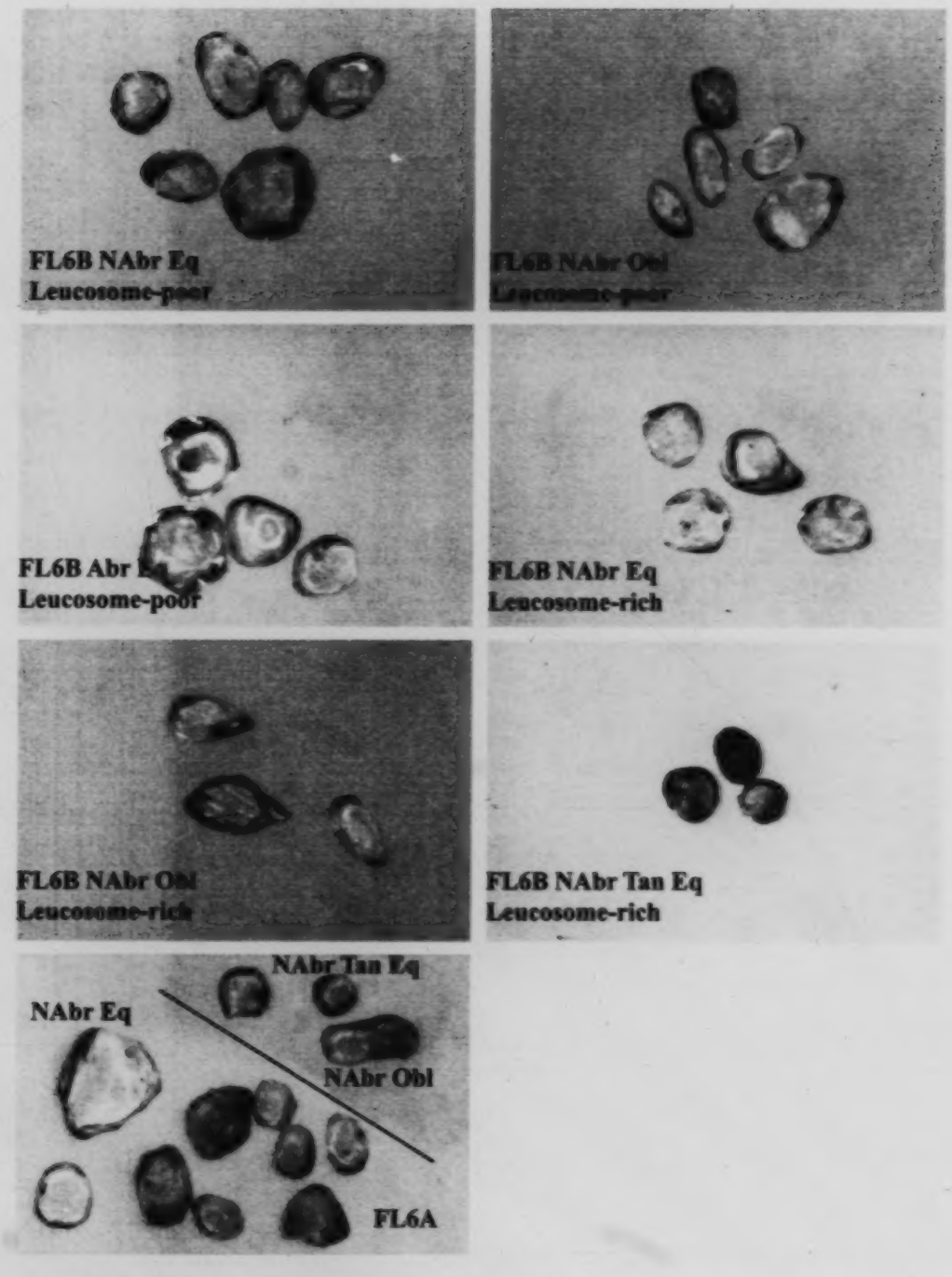

Plate 16. Mafic granulite zircon fractions. Magnification x100. Nabr = non-abraded;

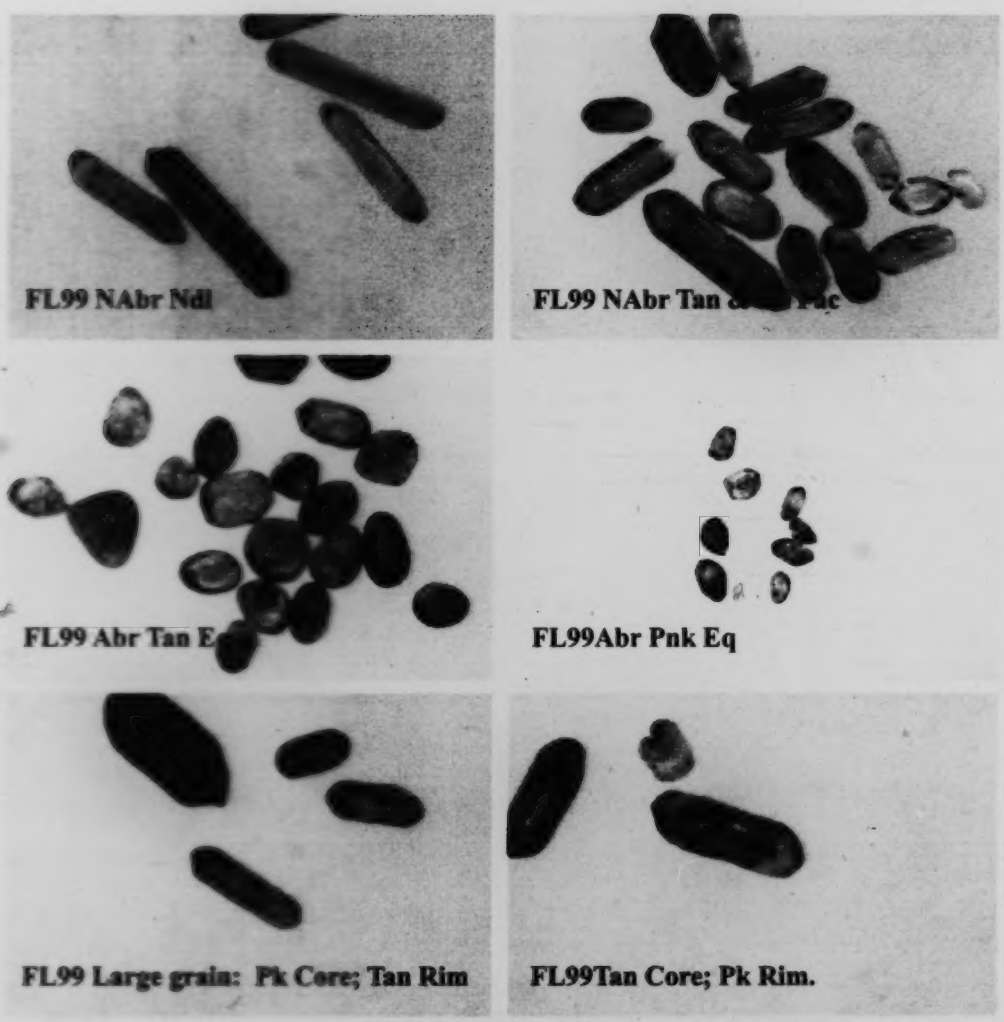

Plate 17. Tonalite zircon fractions. Magnification x100. NABr = non-abraded; Ndl = needle; Fac = faceted; Tan = brown; Pk = pink; Abr = abraded; Eq = equant.

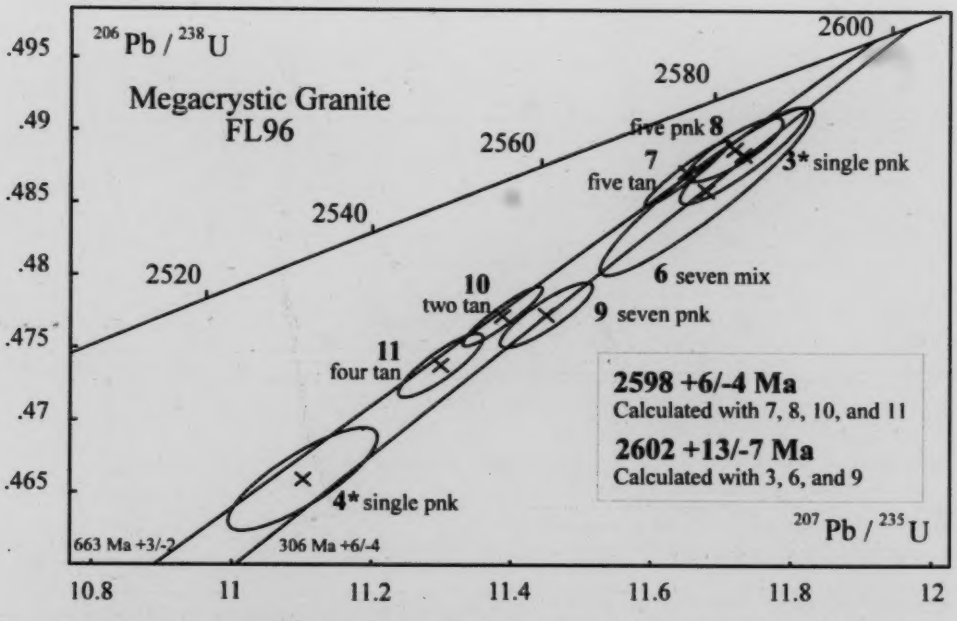

Figure 17. U-Pb concordia diagram for the megacrystic granite zircons, pink (pnk) and brown (tan) fractions. Each analysis is identified by a number that corresponds to the numbering system in Table 5. Ages shown in the inset, lower intercepts values are also given. * Denotes zircon/s *not* abraded.

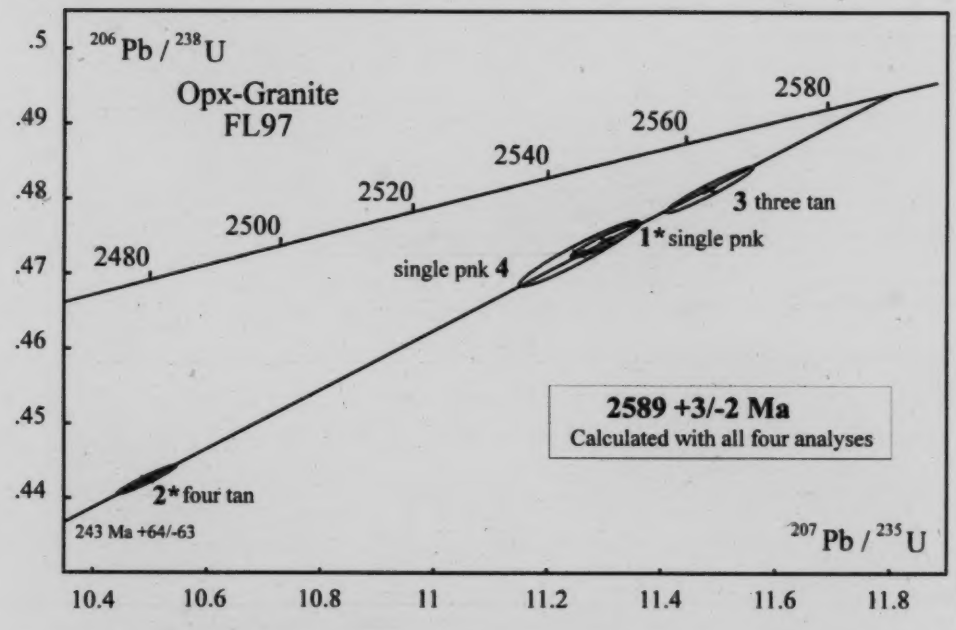

Figure 18. U-Pb concordia diagram for the opx-granite zircons, pink (pnk) and brown (tan) fractions. Each analysis is identified by a number that corresponds to the numbering system in Table 5. The age is shown in the inset, the lower intercept value is also given. * Denotes zircon/s *not* abraded.

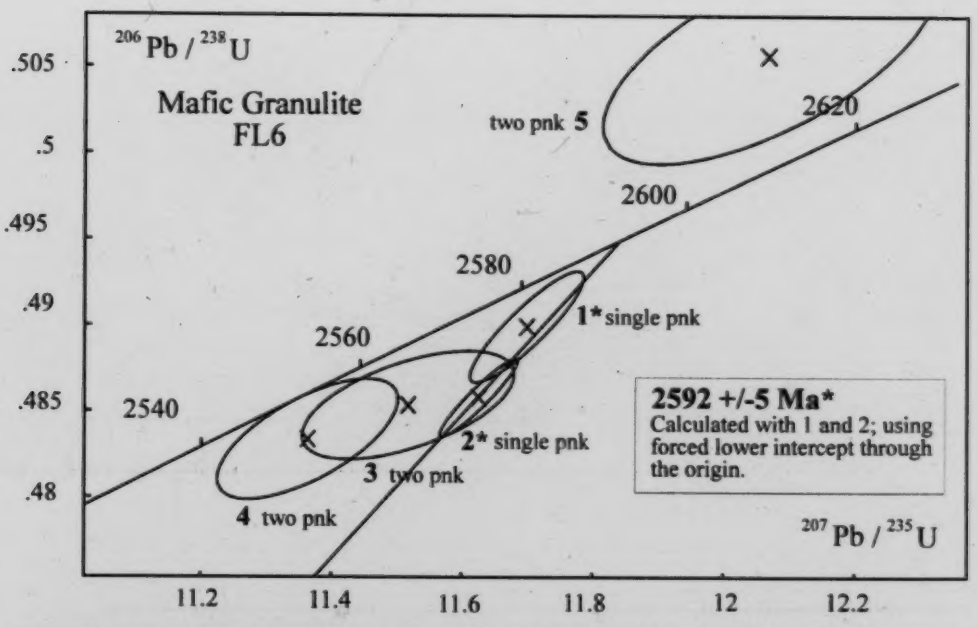

Figure 19. U-Pb concordia diagram for the mafic granulite zircons, pink (pnk) grains. Each analysis is identified by a number that corresponds to the numbering system in Table 5; analyses 1 and 2 (FL6A), analysis 4 (FL6B 'leucosome-rich), and analyses 3 and 5 (FL6B 'leucosome-poor'). Age shown in the inset, the lower intercepts value is also also given. * Denotes zircon/s not abraded.

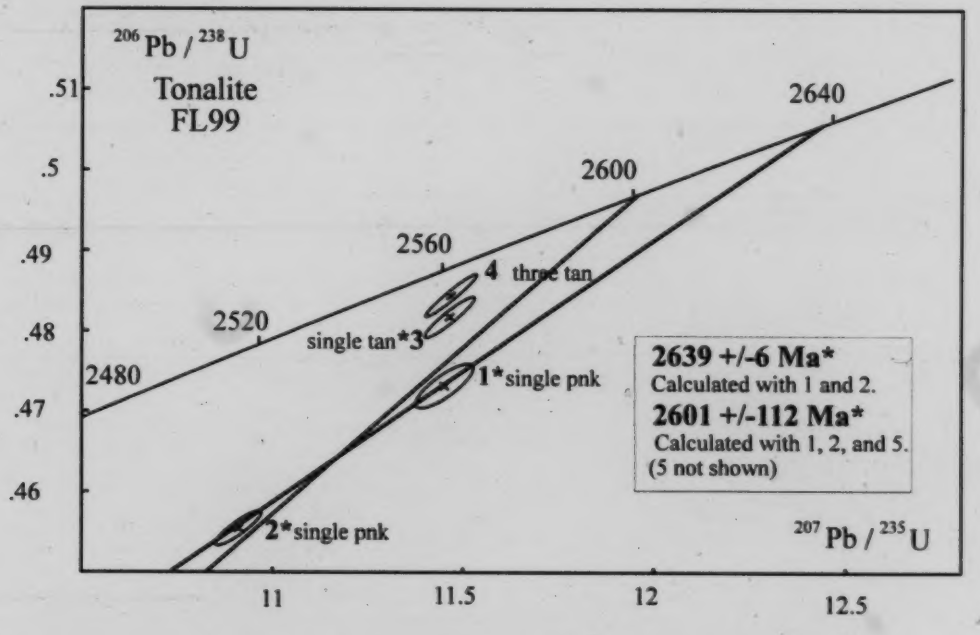

Figure 20. U-Pb concordia diagram for the tonalite zircons, pink (pnk) and brown (tan) fractions. Each analysis is identified by a number that corresponds to the numbering system in Table 5. The age is shown in the inset, the lower intercept value is also given. * Denotes zircon/s *not* abraded.

Table 5. U-Pb zircon results for the Forked Lake megacrystic-granite, opx-granite, tonalite and mafic granulite.

Fraction analysed	Weight	Concentrations (ppm)				Common	Atomic ratios				Apparent ages (Ma)			Discor-
	(mg)	Pb	U	Th	Th/U	Pb (pg)	$^{206}Pb/^{204}Pb$	$^{206}Pb/^{238}U$	$^{207}Pb/^{235}U$	$^{207}Pb/^{206}Pb$	$^{206}Pb/^{238}U$	$^{207}Pb/^{235}U$	$^{207}Pb/^{206}Pb$	dance (%)
								errors * 10^{-5}	errors * 10^{-5}	errors * 10^{-5}				
FL96: Megacrystic Granite														
1 Tan, Fac, NAb,	(1)	0.001	365.33	690.25	179.96	0.261	80.72	284	0.49286±124	11.82273±107	0.17398±141	2583.0	2590.5	2596.3	0.62
2 Tan, Fac, NAb,	(1)	0.003	85.20	116.22	96.25	0.828	50.42	292	0.62538±203	15.01494±150	0.17413±151	3131.3	2816.2	2597.7	-26.02
3 Pnk, Fac, NAb,	(1)	0.003	128.78	226.11	145.16	0.642	15.45	1357	0.48737±117	11.71087± 33	0.17427± 23	2559.3	2581.6	2599.1	1.86
4 Pnk, Equ, NAb,	(1)	0.001	283.72	552.85	213.44	0.386	21.18	778	0.46470±129	11.07487± 41	0.17285± 39	2460.3	2529.4	2585.4	5.82
5 Tan, Equ, NAb,	(1)	0.008	212.24	429.70	13.57	0.032	1032.17	119	0.48513±365	11.71597±291	0.17515±400	2549.6	2582.0	2607.5	2.69
6 Mix, Equ, ABr,	(7)	0.027	100.70	190.72	59.11	0.310	120.88	1333	0.48599±239	11.68400± 62	0.17436± 33	2553.3	2579.4	2600.0	2.17
7 Tan, Equ, ABr,	(5)	0.027	229.06	447.11	76.37	0.171	59.79	5699	0.48735± 92	11.65824± 24	0.17350± 11	2559.2	2577.4	2591.7	1.52
8 Pnk, Equ, ABr,	(5)	0.016	336.22	622.57	239.37	0.384	157.44	1951	0.48895± 91	11.72662± 28	0.17394± 22	2566.1	2582.8	2596.0	1.39
9 Pnk, Equ, ABr,	(7)	0.022	329.07	626.25	230.00	0.367	185.86	2227	0.47749± 92	11.45748± 27	0.17403± 21	2516.3	2561.1	2596.8	3.74
10 Tan, Equ, ABr,	(2)	0.021	670.78	1359.54	170.88	0.126	293.05	2903	0.47466± 91	11.30692± 25	0.17277± 19	2504.0	2548.8	2584.6	3.76
11 Tan, Equ, ABr,	(4)	0.024	499.90	1000.36	160.05	0.160	172.10	9189	0.47682± 85	11.36590± 23	0.17288± 14	2513.4	2553.6	2585.8	3.38
FL97: Opx-Granite															
1 Pnk, Equ, NAb,	(1)	0.004	189.70	384.73	47.66	0.124	25.74	1788	0.47458± 93	11.30288± 24	0.17273± 13	2503.6	2548.4	2584.3	3.77
2 Tan, Equ, NAb,	(4)	0.021	263.98	562.24	120.04	0.214	35.12	9065	0.44248± 80	10.49567± 21	0.17203± 9	2361.7	2479.5	2577.5	9.99
3 Tan, Equ, ABr,	(3)	0.011	330.59	649.37	128.39	0.198	7.03	29549	0.48140±126	11.48550± 31	0.17304± 12	2533.4	2563.4	2587.2	2.52
4 Pnk, Equ, ABr,	(1)	0.008	236.71	477.02	79.37	0.166	43.69	2716	0.47283±180	11.25652± 43	0.172660± 2	2496.0	2544.6	2583.6	4.09
FL99: Tonalite															
1 Pnk, Ndl, NAb,	(1)	0.005	218.38	416.29	164.24	0.395	91.94	661	0.47322±113	11.45046± 31	0.17549± 28	2497.7	2560.6	2610.7	5.22
2 Pnk, Equ, NAb,	(1)	0.003	102.77	211.18	50.22	0.238	21.48	860	0.45550± 89	10.90952± 25	0.17371± 18	2419.6	2515.4	2593.7	8.04
3 Tan, Equ, NAb,	(1)	0.003	357.54	723.25	52.55	0.073	43.09	1683	0.48178±104	11.46393± 27	0.17258± 14	2535.0	2561.6	2582.8	2.24
4 Tan, Equ, ABr,	(3)	0.009	327.47	663.11	32.08	0.048	15.38	11291	0.48448±110	11.46803± 28	0.17168± 11	2546.7	2562.0	2574.1	1.28
5 Pnk, Equ, ABr,	(2)	0.005	39.97	272.12	43.12	0.158	5.60	1777	0.12597± 31	3.04661± 9	0.17541± 27	764.8	1419.4	2609.9	74.76

Table 5. (Continued...)

Fraction analysed	Weight (mg)	Concentrations (ppm) Pb	U	Th	Th/U	Common Pb (pg)	Atomic ratios $^{206}Pb/^{204}Pb$	$^{206}Pb/^{238}U$ errors * 10^{-5}	$^{207}Pb/^{235}U$ errors * 10^{-5}	$^{207}Pb/^{204}Pb$ errors * 10^{-5}	Apparent ages (Ma) $^{206}Pb/^{238}U$	$^{207}Pb/^{235}U$	$^{207}Pb/^{206}Pb$	Discordance (%)
FL6A: Mafic Granulite														
- First Sample - processed whole:														
1 Pnk, Soc, NAb, (1)	0.004	47.73	86.38	42.34	0.490	14.08	832	0.48898±147	11.67739± 45	0.17320± 38	2566.2	2578.9	2588.8	1.06
2 Pnk, TDr, NAb, (1)	0.014	52.43	97.67	37.82	0.387	6.25	6368	0.48580± 93	11.62607± 24	0.17357± 12	2552.5	2574.8	2592.4	1.86
FL6B: Mafic Granulite														
- Processed as leucosome-rich:														
4 Pnk, Soc, Abr, (2)	0.028	8.27	16.04	3.94	0.245	24.39	580	0.48337±143	11.36323± 57	0.17050± 64	2541.9	2553.4	2562.5	0.97
- Processed as leucosome-poor:														
3 Pnk, Soc, ABr, (2)	0.029	8.59	16.81	3.04	0.181	36.03	426	0.48536±129	11.51711± 66	0.17210± 82	2550.6	2566.0	2578.2	1.30
5 Pnk, Obl, ABr, (3)	0.023	3.00	5.66	0.96	0.170	14.04	321	0.50568±257	12.06860±104	0.17309±113	2638.2	2609.8	2587.8	-2.37

Pnk=pink; Tan=brown; Fac=faceted; Equ=equant; Ndl=needle; Soc=soccer-ball; TDr=tear drop; Obl=oblong; NAb=non-abraded; ABr=abraded; all samples Frantz magnetic split at 5° side tilt; number in parentheses represents the total number of grains. The model Th concentration is calculated using the amount of ^{208}Pb present and the U-Pb age. The $^{206}Pb/^{204}Pb$ ratios are corrected for spike and fractionation only while all other atomic ratios are also corrected for blank (see Apendix A for blank values in each case) and initial common Pb using a depleted model Pb isotopic composition (Stacey & Kramer 1975). Blank isotopic composition in University of Alberta laboratory is $^{206}Pb/^{204}Pb=18.3$; $^{207}Pb/^{206}Pb=0.85$; $^{208}Pb/^{206}Pb=2.056$. Values used for Pb (0.088) and U (0.155) fractionations are based on replicate analyses of the SRM*981* Pb (Todt et al. 1996) and U-*500* standards following the Si-gel technique of Cameron et al. (1969). The 1Ó uncertainties listed for the atomic ratios were calculated by propagating all known sources of error including the within run error for all measured isotopic ratios, the uncertainties in fractionation, a ±50% uncertainty in the Pb and U blanks, a ±1% uncertainty in the initial common Pb ratios except $^{207}Pb/^{204}Pb$ (±0.5%), and a ±2% uncertainty in the Pb blank isotopic composition. The decay constants for uranium and the isotopic composition of uranium ($^{238}U/^{235}U=137.88$) used are the values suggested by Jaffrey et al. (1971).

5.3 Discussion of U-Pb Geochronology Results

The upper intercepts of the two granite samples are interpreted as crystallisation ages. The megacrystic granite has a crystallisation age of 2598 +6 -4 Ma and the opx-granite 2589 +3 -2 Ma. These ages are synchronous with three ages for similar granites from the Ghost Lake area, a megacrystic granite at 2598 +3 -2 Ma, an opx-granite at 2589 ±1 Ma, and an undeformed granite at 2593 +6 -4 Ma (Villeneuve and van Breeman 1994). The upper intercept of 2639 ±6 Ma for the tonalite is also interpreted as a tentative age for the crystallisation. This age is poorly constrained but appears to be several tens of million years older than the late plutons. This age is older than a tonalite from the Ghost Lake area with an age of 2605 ±3 Ma (Villeneuve and van Breeman 1994).

The controls on zircon growth under granulite-facies conditions are not well understood (Fraser *et al.* 1997). Mafic metamorphic rocks with igneous protoliths are typically zircon-free at lower grade conditions. However, the reaction hornblende to pyroxene is thought to liberate Zr initiating metamorphic zircon growth during prograde conditions at the transition between upper amphibolite- and granulite-facies (Fraser *et al.* 1997). Thus, zircon in mafic granulites can sometimes be used to obtain a precise age for granulite-facies metamorphism without the complicating effects of zircon inheritance that sometimes plagues similar studies in other rock-types (e.g. metasediments, metagranitoids). The mafic granulite data from FL as it stands, however, present an interesting problem, which only subsequent work on the FL6 zircons may unravel. The existing data are as follows. The FL6 zircons contain evidence for two separate events, an earlier ca. 2592 Ma event broadly synchronous with the intrusion of the opx-granite, represented by analyses FL6A-1 and -2, and a younger event at ca. 2563 Ma, represented by analysis FL6B-4. The existence of two different populations of zircons is supported by the geochemical difference between the two groups. The younger zircons have significantly lower U and Pb concentration and Th/U ratios (Table 5). Presumably, the older zircon population represents zircon growth associated with hornblende breakdown and pyroxene growth - the onset of granulite-facies metamorphism. There is weak

evidence that the younger event also occurred under granulite-facies conditions as analysis FL6B-4 was taken from the leucosome-rich subsample, leucosomes that contain large crystals of orthopyroxene. However, the equant and multifaceted morphologies of most of the FL6 zircons, including those from the leucosome-rich fractionation, suggest growth under melt-absent conditions. In turn, the association of the younger zircons with the leucosome-rich fraction may be coincidental.

Although the thermal conditions of second generation zircon growth are not well constrained, the existence of a younger event is also suggested by the tan fraction of tonalite zircons (Fig. 20), which exhibit $^{207}Pb/^{206}Pb$ ages of 2574 Ma and 2582 Ma. In a first scenario for the interpretation of this fraction, the high U concentration (U ppm = 723, 663) which renders the tan zircons more prone to Pb-loss than their pink counterparts (U ppm = 211, 416), is held responsible for their leftwards shift in position on the concordia diagram during the ca. 2574 / 2582 Ma event. However, if this was the case, one would expect post-metamorphic Pb-loss in the tan fraction to produce more discordant analyses than in the pink fraction (Fig. 20). This is clearly not the case. Therefore, in a second scenario, the tan fraction is attributed to new growth of metamorphic zircon during the ca. 2574 / 2582 Ma event, supported by their distinctly low Th/U ratios (0.048, 0.073), as indicative of metamorphic zircon.

The validity of the younger event may be called into question because of the effect of the laboratory Pb blank and the original common Pb incorporated into analysis FL6B-4. In this case, given the total Pb blank (all non-radiogenic Pb) over a small concentration of radiogenic Pb (Table 5), the assignment of the non-radiogenic between the laboratory and original common Pb provides an inherent uncertainty during the calculation of the U-Pb age. Thus, until further work has been conducted on the FL6B zircons with lower total Pb blanks (currently being undertaken), the validity of the younger event must be regarded as tenuous.

If the ca. 2563 Ma growing event proves to be real, it can be interpreted in terms of three scenarios. In the first scenario, a one-episode history, the evidence suggests a

prolonged period of ~30 Ma in which the mid crust sustained hot thermal conditions punctuated by two periods of zircon growth, one synchronous with the intrusion of the granites at ca. 2592 Ma, and the other at ca. 2563 Ma. Other work has in fact suggested a young age for peak conditions in the deeper crust. Davis (1996, 1997) reports that granulite-facies metamorphism occurred at 2.55 Ga from U-Pb geochronology for metamorphic zircon overgrowths from lower crustal xenoliths. However, if the age of the granulite-facies metamorphism is ca. 2563 Ma, this would 'delay' the intrusion of the FL late pegmatites until this younger event, as field evidence indicates that these magmas intruded into brittle, presumably cooler crust. Magmatic activity of this age is not generally recorded in the majority of the SP, the youngest granitoids in the province are assigned to the Group 3 of Davis *et al.* (1994), and are correlative with rocks between 2600 - 2580 Ma (van Breeman *et al.* 1992). Furthermore, monazite ages of in the range ca. 2580 - 2590 Ma from these granitoids (van Breeman *et al.* 1992), suggest that the crust had cooled significantly subsequent to the ca. 2590 Ma event. Other studies have demonstrated an increasing age gap between radiometric systems with different blocking temperatures with depth. For example, the occurrence of peak conditions at a later date with depth is observed from profiles of radiometric age through the crustal section of the Kapuskasing Uplift, Superior Province (Percival *et al.* 1992 and references therein). The age-depth pattern is interpreted in terms of progressively slower cooling with depth.

In the second scenario, thermal cooling followed the ca. 2592 Ma event and the ca. 2563 Ma zircon growth was promoted by the influx of fluids in the FL under lower-grade conditions. Williams *et al.* (1996), documented zircon ages that post-date the best estimate of peak metamorphism by ~25 m.y. in the Proterozoic Reynolds Range in central Australia, due to a prolonged episode of metamorphic fluid flow. A plausible source for the fluid may be from such intrusions as the leucogranite and pegmatite. Both units provide field evidence supporting late arrival into the FL area and the presence of fluid.

In the third scenario, the ca. 2592 zircons occur in very small melt injections (cryptic in outcrop) originating from the late plutons, rather than zircons hosted by the mafic granulite. However, the morphology of these zircons is typically equant and multifaceted, suggesting growth under melt-absent conditions. This scenario implies that magmatism preceded metamorphism.

The distinction between these three scenarios is currently being explored at the University of Alberta by U-Pb monazite dating. Monazite (~700°C) has a lower closure temperature than zircon (>800°C) (Heaman and Parrish 1991). Therefore, as inferred in the case of the first scenario, if temperatures remained high through the period, the monazite will exhibit a post ca. 2563 Ma age. Alternatively, if the ca. 2592 Ma represents the peak thermal conditions, as is the case in the second scenario, the monazite will likely record an age in excess of 2563 Ma.

6. Conclusions

The first part of this thesis investigated the nature of the deeper crust of the SW SP as exemplified by the FL area, achieved by the presentation of a 1 : 25 000 geology map of the Forked Lake area (Fig. 5), with accompanying lithological and structural descriptions, and incorporating whole-rock geochemical and Nd isotope data for selected rock-types. The second part of this thesis examined the geological and geochronological relationship between igneous activity and high-grade metamorphism in the FL area, using data collected by U-Pb geochronology of zircons. The conclusions of this work are as follows:

- The Nature of the Deep Crust at FL

(1) The FL area is characterised by an early tectono-stratigraphic assemblage composed of metagranitoids and migmatised greywackes, with a subordinate psammitic component. Intruding this assemblage are sills of megacrystic, opx- and leuco-granites, massive to weakly foliated, with abundant sedimentary inclusions.

(2) The geology of the Forked Lake area is exposed in a late-stage dome structure. When the effects of the doming are removed, the geology is composed of a variety of originally flat-lying units and sheet-like intrusions.

(3) The granitoid gneiss is the dominant unit in the area, and is composed of a large proportion of mafic enclaves and layers (10 - 20%) possibly representing transposed and desegregated mafic dykes, and the metagranitoid complex as a whole is thought to represent a deeper level equivalent of the Hinscliffe domain (Henderson and Schaan 1993). The metasediments are more common than previous reconnaissance of the area suggested (Henderson and Chacko 1995), and represent deeper-level equivalents of the YKS, and are compositionally similar to the Burwash Formation.

(4) Granulite-facies metamorphism is represented by the assemblage crd+grt+kfs+melt in the aluminous greywacke, opx+cpx+kfs+pl+qtz+hbl+bt in the

metagranitoids, and hbl+opx+cpx+pl in the mafic granulites, and opx and cpx occur in leucosomes within the metagranitoids. Furthermore, Pehrsson and Chacko (1997) report clinopyroxene and hornblende rims on orthopyroxene, and cordierite rims on garnet, consistent with decompression at high T. Cordierite rimming garnet is also seen in the FL sediment samples.

(5) The metagranitoids and granitoids of the FL area can be classified into the Group 1-3 classification of Davis *et al.* (1994). The late plutons and the tonalite share the geochemical characteristics of the biotite-granites of the Yamba Suite of Group 3, and the metagranitoids are comparable to the Olga Suite of Group 1.

(6) The La_n/Yb_n ratios of the opx-granite are considerably higher ratios than those for the megacrystic granite. These high values indicate a garnet residue in the source area and, coupled with the weakly peraluminous nature of the opx-granite, suggest a meta-igneous source rock of mafic or intermediate composition. As garnet does not develop in such bulk compositions except at much deeper crustal levels (Green 1982), a deeper-level, garnet-bearing source region, and a shallow, garnet-free source region, are suggested for the opx-granite and megacrystic granite, respectively.

(7) The rocks of the FL area have εNd values indicating assimilation or derivation from rocks with depleted mantle model ages between 2.79 and 3.03 Ga. This is consistent with less early Archean material in this part of the western Slave than in the Point Lake area of the northern Slave (Davis *et al.* 1996).

(8) The FL area is characterised by five distinct deformation events (D_1- D_5). These deformation events may be placed in the context of continental thickening (D_1 and D_2) followed by extensional collapse (D_3) of the overthickened zone. Subsequently, the flat lying fabrics of these earlier episodes were tilted to their present pattern by late D_4 - D_5 cross-folding. D_2 is considered to be synchronous with the peak thermal conditions. The switch from compression to extension (D_2 to D_3) was quite short (10 - 15 Ma), suggested by the ductile deformation of D_2 leucosomes by small shear zones. Another set of slightly younger shear zones are suggested by the intrusion of late pegmatite along the

actual site of shear. Both shearing and granite intrusion as part of a regional extension has been proposed for other parts of the central and southern SP (e.g. Davis *et al.* 1994; Stubley 1994).

(9) The geology and structural character of the FL area is similar to the N GD (Henderson and Schaan 1993; Henderson 1994), and the Daran Lake (Pehrsson and Beaumont-Smith 1994; Pehrsson *et al.* 1995) and Snare Lake to Winter Lake regions (Pehrsson and Chacko 1997), located due north of the GD. These high-grade rocks exhibit pronounced high amplitude/short wavelength aeromagnetic anomaly patterns relative to their surrounding lower grade rocks. From these studies and the current study, the distribution of granulite-facies metamorphism can be delineated as a region encompassing a substantial area to the north and south of Ghost Lake. Although large parts of this area, particularly in the GD, are only explored by reconnaissance, the FL is considered to be a lithological representative portion of the GD. Furthermore, the occurrence of a structural dome may be a common feature at this crustal level in this part of the western SP.

- Igneous and Metamorphic Relationships

(10) Geochronological evidence indicates that the granulite-facies metamorphism was broadly synchronous with the intrusion of the opx-granite and megacrystic granites. Thus the late plutons may have provided the primary heat source for metamorphism at this crustal level, or at the very least, augmented existing heat sources. U-Pb zircon analyses on a megacrystic granite at FL yielded an age of 2598 +6 -4 Ma, and for an opx-granite 2589 +3 -2 Ma. The U-Pb analyses correspond to analyses in the N GD on a megacrystic granite with an age of 2598 ±2 Ma, an opx granite at 2589 ±1 Ma, and an undeformed granite of 2593 +6 -4 Ma (Villeneuve and van Breeman 1994). A metamorphic age of ca. 2592 Ma was obtained from metamorphic zircon in a mafic granulite. A younger zircon growth at ca. 2563 Ma is also suggested by the data, and may be related to the influx of fluids into the area, perhaps from the leucogranite and

pegmatites. However, the evidence for this younger event must be considered tenuous, until more precise analyses can be made of the low U, Pb population of zircons in the mafic granulite.

Literature Cited

Bowring, S.A., Williams, I.S., and Compston, W. 1989. 3.96 Ga gneisses from the Slave Province, NWT, Canada. Geology, **17**: 971-975.

Bleeker, W. 1996. Thematic structural studies in the Slave Province, NWT: the Sleepy Dragon Complex. *In* Current research, part C. Geological Survey of Canada, Paper 96-C, pp. 37-48.

Brown, M. 1973. The definition of metatexis, diatexis and migmatite. Proceedings of the Geological Association, vol. 84, p. 371-382.

Cameron, A.E., Smith, D.E., and Walker, R.L. 1969. Mass spectrometry of nanogram size samples of lead. Analytical Chemistry, **41**: 525-526.

Chacko, T., Farquhar, J., and Creaser, R.A. 1995. A petrologic study of granulites and associated rocks from the Ghost Lake area, southwestern Slave Province. Geological Association of Canada / Mineralogical Association of Canada, Program with Abstracts, **20**: A-15.

Cherniack, D.J., Hanchar, J.M., and Watson, E.B. 1997. Rare-earth diffusion in zircon. Chemical Geology, **134**: 289-301.

Creaser, R.B., Erdmer, P., Stevens, R.A., and Grant, S.L. 1997. Tectonic affinity of Nisutlin and Anvil assemblage strata from the Teslin tectonic zone, northern Canadian Cordillera: Constraints from neodymium isotope and geochemical evidence. Tectonics, **16**:107-121.

Davis, D.W. 1982. Optimum linear regression and error estimation applied to U-Pb dating. Canadian Journal of Earth Sciences, **19**:2141-2149.

Davis, W.J. 1996. U-Pb geochronology and Nd isotopic studies of lower crustal xenoliths from the central Slave Province. *In* Slave-Northern Cordillera Lithospheric Evolution (SNORCLE) and Cordilleran Tectonics Workshop Meeting (March 1-3), University of Calgary. *Compiled by* F. Cook, and P. Erdmer. Lithoprobe Report No. **50**, p. 187.

Davis, W.J. 1997. U-Pb zircon and rutile ages from granulite xenoliths in the Slave Province: Evidence for mafic magmatism in the lower crust coincident with Proterozoic dyke swarms. Geology, **25**: 343-346.

Davis, W.J., and Hegner, E. 1992. Nd isotopic evidence for the tectonic assembly of Late Archean crust in the Slave Province, northwest Canada. Contributions to Mineralogy and Petrology, **111**: 493-504.

Davis, W.J., Fryer, B.J., and King, J.E. 1994. Geochemistry and evolution of Late Archean plutonism and its significance to the tectonic development of the Slave craton. Precambrian Research, **67**: 207-241.

Davis, W.J., Gariepy, C., and van Breeman, O. 1996. Pb isotopic composition of late Archean granites and the extent of recycling early Archean crust in the Slave Province, northwest Canada. Chemical Geology, **2033**: 1-15.

Easton, R.M. 1985. The nature and significance of pre-Yellowknife Supergroup rocks in the Point Lake area, Slave Structural Province, Canada. *In* Evolution of Archean

supracrustal sequences. *Edited by* L.D. Ayres, P.C. Thurston, K.C. Card, and W. Weber. Geological Survey of Canada, Special Paper 28, pp. 153-167.

Folinsbee, R.E. 1940. Gem cordierite from the Great Slave Lake area, NWT, Canada. American Mineralogist, **25**: 216.

Fraser, G., Ellis, D., and Eggins, S. 1997. Zirconium abundance in granulite-facies minerals, with implications for zircon geochronology in high-grade rocks. Geology, **25**: 607-610.

Frith, R.A. 1993. Precambrian geology of the Indin Lake map area, District of MacKenzie, Northwest Territories. Geological Survey of Canada, Memoir 424, 63p.

Fyson, W.K., and Helmstaedt, H. 1988. Structural patterns and tectonic evolution of supracrustal domains in the Archean Slave Province, Canada. Canadian Journal of Earth Sciences, **25**: 301-315.

Goldstein, S., O'Nions, R.K., and Hamilton, P.J. 1984. A Sm-Nd isotopic study of atmospheric dust and particulates from major river systems. Earth and Planetary Sciences Letters, **70**: 221-236.

Gorton, M.P. 1977. The geochemistry and origin of Quaternary volcanism in the New Hebrides. Geochem. Cosmochim. Acta, **41**:1257-1270.

Green, T.H. 1982. Anatexis of mafic crust and high pressure crystallisation of andesite. *In* Andesites. Orogenic andesites and related rocks. *Edited by* R.S. Thorpe. John Wiley and Sons, p. 465-487.

Harley, S.L. 1989. The origin of granulites: a metamorphic perspective. Geological Magazine, **126**:215-331.

Heaman, L., Machado, N., and Krogh, T. 1986. Preliminary U-Pb zircon results from the Pikwitonei granulite terrane, Manitoba. Geological Association of Canada / Mineralogical Association of Canada, Program with Abstracts, **11**: A79.

Heaman, L., and Parrish, R. 1991. U-Pb geochronology of accessory minerals. *In* Applications of radiogenic isotope systems to problems in geology. *Edited by* L. Heaman, and J.N. Ludden. Mineralogical Association of Canada Short Course Handbook, Vol. 19, pp. 59-102.

Henderson, J.B. 1970. Stratigraphy of the Yellowknife Supergroup, Yellowknife Bay - Prosperous Lake area, District of MacKenzie. Geological Survey of Canada, Paper 70-26.

Henderson, J.B. 1994. Geology of the Wijinnedi Lake area - a Paleoproterozoic(?) asymmetric uplift of Archean rocks in the southwestern Slave Province, District of MacKenzie, Northwest Territories. *In* Current research, part C. Geological Survey of Canada, Paper 94-C, pp. 71-79.

Henderson, J.B., and Schaan, S.E. 1993. Geology of the Wijinnedi Lake area, a transect into mid-crustal levels in the western Slave Province, District of MacKenzie, NWT. *In* Current research, part C. Geological Survey of Canada, Paper 93-C, pp. 83-91.

Henderson, J.B., and Chacko, T. 1995. A record of the high grade terrane south of Ghost Lake, southwestern Slave Province, NWT. *In* Current research, part C. Geological Survey of Canada, Paper 95-C, pp. 77-85.

Hill, J.D., and Frith, R.A. 1982. Petrology of the Regan Intrusive Suite in the Nose Lake-Beechey Lake map area, District of MacKenzie. Geological Survey of Canada, Paper 82-8, pp. 1-26.

Hoffman, P.F. 1989. Precambrian geology and tectonic history of North America. *In* The Geology of North America- an overview. *Edited by* A.W. Bally, and A.R. Palmer. Geological Survey of America, pp. 447-512.

Holland, T.H. 1900. The charnockite series, a group of Archean hypersthenic rocks in peninsular India. Geological Survey of India, Memoir 2, pp. 192-249.

Hooper, P.R., Johnson, D.M., and Conrey, R.M. 1993. Major and trace element analyses of rocks and minerals by automated X-ray spectrometry. Open File Report, Washington State University, Pullman, Washington.

Irvine, T.N., and Baragar, W.R.A. 1971. A guide to the chemical classification of the common volcanic rocks. Canadian Journal of Earth Sciences, **8**: 523-548.

Jaffrey, A.H., Flynn, K.F., Glendenin, L.E., Bentley, W.C., and Essling, A.M. 1971. Precision measurement of half-lives and specific activities of ^{235}U and ^{238}U. Physics Review, **4**: 1889-1906.

James, D.T., and Mortensen, J.K. 1992. An Archean metamorphic core complex in the southern Slave Province: basement cover structural relations between the Sleepy Dragon Complex and the Yellowknife Supergroup. Canadian Journal of Earth Sciences, **29**: 2133-2145.

Knaack, C., Cornelius, S., and Hooper, P. 1994. Trace element analyses of rocks and minerals by ICP-MS. Open File Report, Washington State University, Pullman, Washington.

Kretz, R. 1973. Symbols for rock-forming minerals. American Mineralogist, **68**: 277-279.

Krogh, T.E., and Gibbins, W. 1978. U-Pb isotopic ages of basement and supracrustal rocks in the Point Lake area of the Slave Structural Province, Canada. Geological Association of Canada, Program with Abstracts, **3**: 438.

Kusky, T.M. 1989. Accretion of the Archean Slave Province. Geology, **17**: 63-67.

Lord, C.S. 1942. Snare River and Ingray Lake map-areas, Northwest Territories. Geological Survey of Canada, Memoir 235.

Ludwig, K.R. 1996. A plotting and regression program for radiogenic isotope data. U.S. Geological Survey, Open File Report, 91-445.

Maniar, P.D., and Piccoli, P.M. 1989. Tectonic discrimination of granitoids. Geological Society of America, Bulletin 101, pp. 635-643.

Morris, G.A., and Hooper, P.R. 1997. Petrogenesis of the Colville Igneous Complex, northeast Washington: implications for Eocene tectonics in the nothern U.S. Cordillera. Geology, **25**: 831-834.

Padgham, W.A. 1985. Observations and speculations on supracrustal sequences in the Slave Structural Province. *In* Evolution of Archean supracrustal sequences.

Edited by L.D. Ayres, P.C. Thurston, K.C. Card, and W. Weber. Geological Association of Canada, Special Paper 28, pp. 133-152.

Padgham, W.A., and Fyson, W.K. 1992. The Slave Province: a distinct Archean craton. Canadian Journal of Earth Sciences, **29**: 2072-2086.

Parrish, R.R. 1990. Cooling rates from 700°-400° in high grade rocks: applications of U-Pb geochronometry. V.M. Goldschmidt Conference, Program and Abstracts, **72**.

Pearce, J.A. 1983. Role of the sub-continental lithosphere in magma genesis and continental margins. In Continental Basalts and Mantle Xenoliths. *Edited by* C.J. Hawkesworth and M.J. Norry. Cambridge, Mass., pp. 230-249.

Pearce, J.A., and Cann, J.R. 1973. Tectonic setting of basic volcanic rocks investigated using trace element analyses. Earth and Planetary Sciences Letters, **19**: 290-300.

Pearce, J.A., Harris, N.B.W., and Tindle, A.G. 1984. Trace element discrimination diagrams for the tectonic interpretation of granitic rocks. Journal of Petrology, **25**: 956-983.

Pearce, J.A., Baker, P.E., Harvey, P.K., and Luff, I.W. 1995. Geochemical evidence for subduction fluxes, mantle melting and fractional crystallisation beneath the South Sandwich Island arc. Journal of Petrology, **36**:1073-1109.

Peccerillo, A., and Taylor, S.R. 1976. Geochemistry of Eocene calc-alkaline volcanic rocks from the Kastamonu area, northern Turkey. Contributions to Mineralogy and Petrology, **58**:68-81.

Pehrsson, S.J., and Beaumont-Smith, C. 1994. Preliminary report on the geology of the Indin Lake supracrustal belt, western Slave Province, Northwest Territories. *In* Current research, part C. Geological Survey of Canada, Paper 94-C, pp. 91-102.

Pehrsson, S.J., Grant, J.W., Dorval, A.C., and Lewis, M. 1995. Structure and stratigraphy of the Indin Lake area, western Slave Province, Northwest Territories. *In* Current research, part E. Geological Survey of Canada, Paper 95-E, pp. 49-159.

Pehrsson, S.J., and Chacko, T. 1997. Contrasting styles of deformation and metamorphism between mid and upper crustal rocks of the western Slave Province, Northwest Territories. *In* Current research, part C. Geological Survey of Canada, Paper 97-C, pp. 15-25.

Percival, J.A., and Krogh, T.E. 1983. U-Pb zircon geochronology of the Kapuskasing structural zone and vicinity in the Chapleau-Foleyet area, Ontario. Canadian Journal of Earth Sciences, **20**: 830-843.

Percival, J.A., Fountain, D.M., and Salisbury, M.H. 1992. Exposed crustal cross sections as windows on the lower crust. *In* Continental Lower Crust. *Edited by* D.M. Fountain, R. Arculus, and R.W. Kay. Developments in Geotectonics 23, Elsevier, pp. 317-362.

Pichamuthu, C.S. 1969. Nomenclature of charnockites. Indian Mineralogist, **10**: 23-25.

Robertson, D.K., and Folinsbee, R.E. 1974. Lead isotope ratios and crustal evolution of the Slave craton at Ghost Lake, NWT. Canadian Journal of Earth Sciences, **11**: 819-827.

Shand, S.J. 1947. Eruptive Rocks. Their Genesis, Composition, Classification, and their Relation to Ore-Deposits. 3rd ed. John Wiley and Sons, New York.

Shervais, J.W. 1983. Ti/V plots and the petrogenesis of modern and ophiolitic lavas. Earth Planetary Science Letters, **59**:101-108.

Silver, L.T., and Chappell, B.W. 1988. The Peninsular Ranges Batholith: an insight into the evolution of the Cordilleran batholiths of southwestern North America. Transactions of the Royal Society of Edinburgh, **79**:105-121.

Stacey, J.S., and Kramer, J.D. 1975. Approximation of terrestrial lead isotope evolution by a two-stage model. Earth and Planetary Sciences Letters, **26**: 207-221.

Stern, R.A., Bleeker, W., and Theriault, R.J. 1997. U-Pb SHRIMP zircon chronology of 4.02 Ga tonalite, Acasta Gneiss Complex, NWT, Canada. Geological Association of Canada / Mineralogical Association of Canada, Program with Abstracts, 22: A142.

Stubley, M.P. 1994. High-grade supracrustal rocks in the Nardin Lake area, south-central Slave Province (85 0 & P). Yellowknife Geoscience Forum, 56-57.

Taylor, S.R., and McLennan, S.M. 1985. The continental crust: its composition and evolution. Blackwell, Oxford.

Thompson, P.H. 1978. Archean regional metamorphism in the Slave Structural Province- a new perspective on some old rocks. *In* Metamorphism in the Canadian Shield. Geological Survey of Canada, Paper 78-10, pp. 85-102.

Thompson, P.H., Ross, D., Froese, E., Kerswill, J.A., and Peshko, M. 1993. Regional geology in the Winter Lake - Lac de Gras area, central Slave Province, District of MacKenzie, Northwest Territories. *In* Current research, part C. Geological Survey of Canada, Paper 93-1C, pp. 61-70.

Thompson, P.H., Ross, D., and Davidson, A. 1994. Regional geology of the Winter Lake - Lac de Gras area, central Slave Province, District of MacKenzie, Northwest Territories. *In* Current research, part C. Geological Survey of Canada, Paper 94-C, pp. 1-12.

Thorpe, R.I., Cumming, G.L., and Mortensen, J.K. 1992. A significant Pb isotope boundary in the Slave Province and its probable relation to ancient basement in the western Slave Province. *In* Project Summaries, Canada- NWT Mineral Development Agreement 1987-91. Geological Survey of Canada, Open File 2484, pp. 179-184.

Todt, W., Cliff, R.A., Hanser, A., and Hofmann, A.W. 1996. Evaluation of ^{202}Pb-^{205}Pb Double Spike for High-Precision Lead Isotopic Analysis. *In* Earth Processes, Reading the Isotopic Clock. *Edited by* A. Basu, and S. Hart. Geophysical Monograph 95, pp. 429-437.

van Breeman, O., Davis, W.J., and King, J.E. 1992. Temporal distribution of granitoid plutonic rocks in the Archean Slave Province, northwest Canadian Shield. Canadian Journal of Earth Sciences, **29**: 2186-2199.

van der Mølen, I., and Paterson, M.S. 1979. Experimental deformation of partially-melted granite. Contributions to Mineralogy and Petrology, **70**:299-318.

Villeneuve, M., Jackson, V.A., and Thompson, P.H. 1993. Geochronological evidence for the existence of pre-Yellowknife Supergroup supracrustal sequences in the

Slave Province. Geological Association of Canada, Program with Abstracts, 18: A107.

Villeneuve, M., and van Breeman, O. 1994. A compilation of U-Pb data from the Slave Province. Geological Survey of Canada, Open File 2972, 53p.

Williams, I.S., Buick. I.S., and Cartwright, I. 1996. An extended episode of early Mesoproterozoic metamorphic fluid flow in the Reynolds Range, central Australia. Journal of Metamorphic Geology, **14**: 2947.

Wright, G.M. 1954. Ghost Lake, District of MacKenzie, NWT. Geological Survey of Canada, Map 1021A.

Yardley, D.H. 1949. Wecho River (east half), NWT. Geological Survey of Canada, Paper 49-14, scale 1:126-720.

Yardley, W.D. 1989. An introduction to metamorphic petrology. Longman Scientific and Technical, 248p.

Appendix A

Locations of Samples

Forked Lake 115°15' 63°40'

Sample	UTM co-ordinates
FL1	585474-7058022*
FL45A	586000-7060700
FL49B	588300-7060400
FL68A	587500-7060000
FL2A	585377-7058171*
FL2B	585377-7058271*
FL5A	586756-7060179*
FL28	585500-7058000
FL40	585700-7061500
FL98	585600-7058000
FL20A	586700-7059300
FL84A	590200-7060200
FL6A	586882-7060925*
FL82B	587600-7059000
FL24	587573-70590234*
FL74	590212-7059257*
FL52	588700-7059900
FL82A	587600-7059000
FL96	588124-7059595*
FL10A	587902-7060060*

*GPS co-ordinates (North American Datum); otherwise calculated from grid co-ordinates.

APPENDIX B

Cleaning Procedures

Teflon bombs: Between each sample run, the Teflon™ bombs were cleaned in four cycles, spending 2 days in the oven for each step, in the following sequence:

1. ~15 drops 48% HF and ~2 drops 7.0N HNO_3
2. ~30 drops 6.0N HCl
3. ~15 drops 48% HF and ~2 drops 7.0N HNO_3
4. ~15 drops 48% HF and ~2 drops 7.0N HNO_3

Isotope chemistry beakers: The beakers used to collect the U and Pb elution from the mini columns were prepared as follows:

1. 6.0N HCl bath 1 hour (~60°C).
2. Hot plate (~60°C) with 7.0N HNO_3, for 3 hours.

Mini-column & resin cleaning:

1. Mini-columns stored in 6.2N HCl tub.
2. Resin added to mini-column, and cleaned by 3-5 passings of millpore, then 3-5 sequences 6.2N HCl.